Composites Part B 244 (2022) 110148

Contents lists available at ScienceDirect

Composites Part B

journal homepage: www.elsevier.com/locate/compositesb

Rheological model of fresh concrete considering granular characteristics

Zhuguo Li

Graduate School of Science and Technology for Innovation, Yamaguchi University, Ube, Yamaguchi, Japan

ARTICLE INFO

Keywords:
Fresh concrete
Interfriction
Yield stress
Rheology
Thixotropy
Viscoelasticity
Viscoplastic flow
Viscous granular fluid

ABSTRACT

In this paper, the microscopic approach was proposed to clarify the rheological behaviors of fresh concrete, which treats fresh concrete as a granular fluid with viscousness and inter-particle friction, and gets the shear deformation of fresh concrete by accumulating the particle motions in the shear direction. After investigating the probability of occurrence of moving particles, average particle contact angle, and average particle movement distance under shear stress, constitutive equations of fresh concrete before and after yielding were derived, and dynamic yield stress model, viscoelastic deformation model and viscoplastic flow model were obtained, respectively. The numerical calculations confirmed that these models can describe the complex rheological behaviors of fresh concrete presenting in the rheological experiments, including viscoelastic deformation before yielding, non-linearity of viscoplastic flow, shear thinning, and the dependence on normal stress and shear history.

1. Introduction

Workability of concrete is a broad and subjective term describing how easily fresh concrete can be transported, placed, consolidated, and finished with minimal loss of homogeneity. Japanese Architectural Standard Specification (JASS 5) states that concrete should be placed densely inside formwork and around rebars with little segregation [1]. Thus, the workability of concrete depends on rebar arrangement of concrete member, transportation distance and method, and placement method, not only its consistency. That is, the concrete should have appropriate flowability and segregation resistance in accordance with the construction method and structural condition of reinforced concrete.

Due to the use of mineral and chemical admixtures, fresh concrete has become so complex and diverse that slump and slump flow value are not enough to accurately evaluate its properties. In addition, to ensure the seismic performance of buildings or in high-rise concrete structures, the steel reinforcement is densely arranged, which increases the difficulty of concrete placement. Workability evaluation and optimization, hereafter called workability design, has become important, considering the construction method and structural condition of reinforced concrete. The empirical tests, such as the slump test and the L-flow test, measure a value specific to respective test method, thus may not be sufficient to ensure the adequate performances for the various construction steps (pumping, casting, formwork pressure, etc.) because different aspects of workability are not described. The workability design can be done through construction experiment of concrete, e.g. pumping experiment, but the experiments are time and labor intensive.

Rheology is an effective tool for managing and achieving the workability of fresh concrete and the mechanical performance of hardened concrete [2]. In addition, the design and improvement of cement-based 3D printing materials need to be based on their rheological properties [3–5]. Concrete workers may have a good understanding of the workability of concrete with a certain slump value, but they do not always know what a certain rheological test result means. In order to use the rheology of concrete in practice, it is necessary to relate the rheological parameters to concrete workability. In 1988, Tanigawa extended the traditional objective of the rheology of fresh concrete from the property evaluation to the workability design that is based on numerical flow simulation [6], called numerical workability design here. In contrast to the property evaluation, which requires as few easily measurable indexes as possible, effective numerical flow simulation requires accurate rheological model and comprehensive input parameters.

Since Tattersall [7] proposed the two-point workability test method, most of the rheological studies of fresh concrete have regarded fresh concrete as a Bingham material. As a simple model, the Bingham model has been widely used to describe approximately the viscoplastic flow behavior of fresh cement-based materials, as shown in Eq. (1.1). However, the Bingham model has three drawbacks for describing fluids in general [8]. First, flow curves (the $\tau - \dot{\gamma}$ relational curves) are rarely linear in reality. Second, flow hysteresis often occurs when measuring ascending and descending flow curves. Third, the Bingham yield stress is not a well-defined property.

E-mail address: li@yamaguchi-u.ac.jp.

https://doi.org/10.1016/j.compositesb.2022.110148
Received 25 November 2021; Received in revised form 8 July 2022; Accepted 20 July 2022
Available online 8 August 2022

$$\tau = \tau_b + \eta\dot{\gamma} \quad \tau \geq \tau_b$$

$$\dot{\gamma} = 0 \qquad \tau < \tau_b \tag{1.1}$$

where, τ is shear stress, $\dot{\gamma}$ is shear strain rate, τ_b is Bingham yield stress, and η is plastic viscosity.

Even fresh cement paste and high fluidity concrete always show nonlinear flow behaviors [9–11]. The linear Bingham equation may be an acceptable equation over a narrow range of low shear rates [8,12]. Self-compacting concrete (SCC) only shows the Bingham fluid behavior in the shear rate range 0–10 s^{-1} applicable for regular casting operations except mixing and pumping [13]. Non-linear flow curve of SCC would result in apparently negative yield stress when the Bingham model is applied [11]. Since the flow curve of fresh concrete is not a straight line, the measured result of plastic viscosity depends on the range of flow curve and the magnitudes of shear rates chosen to determine the Bingham constants [12]. Compared to fresh concrete containing coarse aggregate, the rheological behaviors of cement paste seem to be easier to measure accurately with rheometers, thus many nonlinear flow models have been proposed, such as the Modified Bingham model [14].

The non-linear behavior of fresh cement-based materials usually shows the shear thinning [10,15], which is generally explained to be due to the shear-induced breakdown of the flocculated structure of particles [2,16]. The shear stress decreases with shearing time, i.e., the stress relaxation, and the decrease of apparent viscosity and yield stress with shearing time over a short timescale is also a result of the time-dependent breakdown of the flocculated structure [17–19]. While over a large timescale, rebuilding of the de-flocculated structure may cause fresh cement-based materials to show the shear thickening behavior due to physical flocculation and cement hydration [19,20]. Therefore, the rheological properties of fresh cement-based materials vary with shearing time, i.e. depending on the stress duration or shear history. Feys et al. found that SCC is a shear thickening material, but the mechanism has been yet unclear [11]. The Herschel-Bulkley model has been recommended to describe the non-linear flow behaviors recently [9,10], which is presented as a combination of the Bingham and Power models, as shown in Eq. (1.2).

$$\tau = \tau_0 + a\dot{\gamma}^b \tag{1.2}$$

where τ_0 is yield stress, a is the consistency, and b is the power index that represents the deviation from a Bingham behavior: $b > 1.0$ represents the shear thickening flow, and $b < 1.0$ represents the shear thinning flow.

It is difficult to quantitatively investigate the breakdown of the flocculated structure of particles. Thus, Li et al. discussed theoretically the nonlinear constitutive equation of high fluidity concrete based on the Eyring's rate process theory about shear flow of matter [12]. The number of the moving cement particles, leading to the time-dependent flow of fresh concrete, increases as a hyperbolic function of shear stress. The flow curve equation of high fluidity concrete with the characteristic of shear thinning was obtained, as shown in Eq. (1.3). This theoretical result confirmed the Vom Berg model obtained through the rheological experiments of cement pastes [21], and clarified the influencing factors of the model equation's parameters.

$$\dot{\gamma} = c_x \sinh\left[c_y(\tau - \tau_0)\right] \tag{1.3}$$

where c_x and c_y are constants related to environmental temperature and the number of cement particle, and τ_0 is yield stress depending on mean inter-particle frictional angle, normal stress, and surface tension of water.

Fresh concrete consists of solid particles and water, so called viscous granular fluid. Stiff concrete should be strictly called granular material or particle assembly rather than fluid or suspension. Dense suspensions share the same complex features due to the wide variety of interactions (colloidal, hydrodynamic, frictional, collisional, etc.) between the particles [22]. In cement paste at a high plasticizer concentration, all cement particles are supposed to be completely suspended in the balance of van der Waals attractive force, electrostatic repulsion force, and gravity. However, it is not realistic that in fresh concrete there is no cement particle flocculation and solid particle contact at all [23]. The increase in the volume fraction of solid particles causes the direct contacts between the particles to become important, and the maximum volume fraction is the limit of application of models considering only hydrodynamic interactions between the particles [24]. Friction should occur between the solid particles in contact, which fulfills Coulomb's friction law, and is one of the factors causing yield stress and normal stress-dependence of shear flow [12,25,26]. Mori & Tanigawa found in the shear experiments that the shear resistance of fresh concrete depends on the external vertical pressure acting on the surface of concrete sample, and further proposed a vertical pressure-dependent model, as shown in Eq. (1.4), in which the Bingham constants are proportional to the normal stress induced by external vertical pressure [27].

$$\tau = \dot{\gamma}(\eta_n\sigma_{ne} + \eta_0) + (\tau_n\sigma_{ne} + \tau_0) \tag{1.4}$$

where σ_{ne} is normal stress caused by external vertical pressure, τ_0,η_0 are yield stress and plastic viscosity at $\sigma_{ne} = 0$, respectively, and τ_n, η_n are proportional coefficients.

The fact that fresh concrete can stand without flowing under its own gravity suggests that the minimum stress, known as yield stress, is necessary to initiate a flow, and thus conventional concrete is considered to be a yield stress fluid and to have solid-like behavior below the yield stress [28,29]. Although some experiments showed that SCC has a small yield stress near zero, and thus approaches to the behavior of Newtonian or power-law fluid [8], fresh cement-based materials are still classified as non-Newtonian granular fluids. The yield stress is a macroscopic counterpart of the friction between solid particles and is interpreted as the stress necessary to apply in order to overcome the inter-granular contact forces [28]. The water surface tension also increases the yield stress [25]. The static yield stress is generally used as the indication of yield stress because it is associated with the beginning of liquid-like behavior - that is, starting from a static state and going to a dynamic state (going from rest to flow) [2]. The static yield stress is related to the particle flocculation at rest and the particle de-flocculation under flow. Because the links between particles can be broken by shearing, the measured yield stress depends upon shearing time and previous shear history [16]. Roussel suggested that the static yield stress or called apparent yield stress is a function of shear rate and its elapsed time, and further proposed a thixotropic model of shear resistance, as shown in Eq. (1.5) [30].

$$\tau = (1 + \lambda_0 e^{-\alpha\dot{\gamma}t})\tau_0 + \eta\dot{\gamma} \tag{1.5}$$

where, α is proportional coefficient, λ_0 is initial flocculation state of the material, t is elapsed time, and τ_0 is initial yield stress.

Basically, fresh cement-based materials exhibit a non-linear viscoelastic behavior at a lower shear stress than the static yield stress [8,31–34]. Formwork pressure during conventional concrete construction and elastic buckling during 3D concrete printing are related to the elasto-plasticity and the yield stress [28,35]. In addition, the prediction of coarse aggregate settlement and the flow blockage in pumping pipe or between reinforcing bars requires understanding of the viscoelastic deformation behavior of matrix mortar or fresh concrete. However, rheological researches of fresh concrete have focused on the static yield stress that finally determines the flow length or the filling degree of a mold, and the apparent viscosity that is associated with the filing speed in a mold, the viscoelastic behavior has not yet fully clarified and modeled.

On the other hand, there are many rheometers proposed for the rheological measurement of fresh concrete, such as Coaxial Cylinder Rheometer (BML), Parallel Plate Rheometer (BTRHEOM), Impellers Rheometer (e.g. IBB, Two-Point Rheometer), Vane-In Cup Rheometer (e.

g. ICAR rheometer) [8], and Shear Box [27]. Although the rheological measurement by any of the rheometers is not as easy as the slump test, the rheometers are more reasonable to evaluate the properties of fresh concrete by two parameters than the slump value only. However, almost of all the rotational rheometers are basically designed to measure the Bingham constants (Bingham yield stress, plastic visocity) of fresh concrete by shear rate ($\dot{\gamma}$)-controlled method, but are not well-suited for stiff concrete. Bingham yield stress is also called dynamic yield stress [2]. Since dynamic yield stress is determined on basis of the "down" flow curve, it should not be larger than the static yield stress. Thus, the difference between the static yield stress and the Bingham yield stress was used to quantify the thixotrop of fresh mortar [36]. Though a rate-controlled stress growth test is recommended to measure the shear stress-shear strain (or time) relationship for determining the static yield stress [2], this test method is currently found to be most used only for cement pastes [28,37]. This is because that the rotational rheometers are not capable of rotating at sufficiently low rotational speeds for fresh concrete [8], and the measurement accuracy is low due to the end-effect, the wall-slip and the sedimentation of aggregate as explained later. For this reason, a creep-recovery protocol was used to measure the static yield stress of fresh mortar [36].

It is almost impossible to use current rotational rheometers to measure the shear stress-shear strain relationship of fresh concrete for investigating the viscoelastic deformation behavior before yielding. Even for the measurement of the viscoplastic flow behavior after yielding, there are also many problems. The problem of plug flow, i.e. dead zone, was first raised by Tattersall and Dimond [38], but has never been satisfactorily resolved [16]. Since the gap between rotor and stator must be large enough to guarantee laminar and homogeneous flow of fluid [14], and since coarse aggregate poses difficulties in measurement, the rheological measurements using small size apparatus are not reliable. Moreover, even when using the cylinders or the plates with roughened surfaces, it is not yet certain that the wall-slip will not occur at all on the roughened surfaces [16].

Segregation (bleeding and particle sedimentation) is one of the most important factors that reduce the reliability of rheological measurement of fresh cement-based materials. Gravitational sedimentation causes to overestimate the yield stress and the plastic viscosity, though the angled blades of the impeller rheometer may lift the particles to keep the sample homogeneous only to a certain extent [39]. In the gap of parallel plate rheometer, sedimentation leads to a layer of bleeding water under the upper plate, which causes the problem of wall-slip [16]. Wallevik [40] found that radial migration of coarse particles in concrete, called centrifugal separation, results in a lower measured yield stress and the no-linearity of flow curve. Overall, segregation leads to changing rheological properties of the material during measurement, and makes the rheological test results very difficult to interpret [13].

The rheological test results also depend on the sample dimension of fresh concrete that influences gravity-induced normal stress [12]. In addition, since fresh concrete is a highly concentrated suspension, particle sliding past each other leads to an expansion in volume during shearing, i.e. dilatancy [8]. It is yet unclear that fresh concrete having what level of fluidity will exhibit dilatancy, but the rheological behaviors of low/middle fluidity concretes are possibly influenced whether the dilatancy is constrained or not [41,42]. The potential dilatancy is constrained by the cylinders or the plates of rotational rheometers. These complex influencing factors make the test results of concrete rheometers have low accuracy and repeatability, and the test results of different rheometers are not consistent in absolute terms [2,43]. Also, for the impellers rheometer and the vane-in-cup rheometer, it is generally not possible to convert the measured torque and rotation speed values to constitutive equation parameters. Complex calculation is needed for getting the τ–$\dot{\gamma}$ relationship [44], or the Bingham constants are delivered by using the calibration coefficients [45].

Therefore, it is extremely difficult to clarify the rheological behaviors of fresh concrete with precision by rheological experiments. So far, many experiments on fresh concrete have been limited to qualitative investigation for given mixtures, lacking systematicity and universality, thus the findings have rarely been referenced by the studies of other fluids or materials.

As mentioned above, several rheological models have been proposed for fresh concrete, but none of them is widely applicable to concretes ranging from stiff to high fluidity types, and can also fully describe the complex rheological behaviors before and after yielding. In order to realize the numerical workability design of fresh concrete, it is essential to establish an accurate constitutive model that treats with the granular feature of fresh concrete in addition to its fluid feature. In view of the difficulties of experimental investigation, the author suggested to study constitutive law of fresh concrete using the microscopic approach, where macroscopic deformation and flow behaviors of fresh concrete are derived from the movement of particles. This kind of microscopic approach was first successfully used to clarify the mechanical behavior of soil [46]. The author proposed a multiphase model of fresh cement-based materials, and expanded the Eyring's rate process theory to make it applicable to viscous granular fluid, following by the clarification of the shear deformation mechanism of fresh cement-based materials [47]. In the multiphase model, fresh cement-based materials are regarded as concentrated granular fluid consisting of water, viscous binder particles, and non-viscous aggregate particles. The solid particles have inter-fiction, the tightness of particle configuration is represented by average value of particle contact angles (PCA), and the surface tension of water causes an increase in the interparticle friction. Base on the multiphase model and the shear deformation mechanism, the microscopic approach was proposed for fresh cement-based materials. The microscopic approach has been used to investigate theoretically the constitutive model [12], the yield stress model [25], and the thixotropic behaviors [20] of high fluidity concrete, as well as the rheological model of fresh concrete in vibrated state [48]. In this study, taking both the fluid feature and the granular characteristic of fresh concrete into account, the author further discussed the universal constitutive models of fresh concretes ranging from stiff to high fluidity types, for describing the viscoelastic deformation behavior before yielding and the viscoplastic flow behavior after yielding, respectively.

2. Experimental investigations on shear deformation and flow models

There have already been many rheological experiments to investigate the viscoplastic flow of fresh cement-based materials after yielding. The viscoplastic flow is shear-thinning in most cases, but SCC with small water-binder ratio or large slump flow, or at high shear rates, shows the shear-thickening behavior [11,13]. However, little investigation has been carried out so far on the viscoelastic deformation behavior before yielding. Uzomaka [49] and Koehler et al. [8] measured the torque-shear deformation relationship by the rate-controlled method, and explained that the peak torque was attributed to the formation and breakdown of the internal structure of fresh concrete. The peak shear stress was also found in the shear stress (τ) -shear strain (γ) relational curve of cement paste measured at a small constant shear rate, and the τ–γ relational curve before the peak shear stress can be divided into rapid increase phase and slow increase phase [33].

The stress-controlled stress growth test measures the free deformation response to shear stress, while the rate-controlled stress growth test records the resulting stress of a forced deformation at a constant shear rate. During the concrete construction, fresh concrete deforms or flows under gravity, and vibration force or pumping pressure. Hence, the former test is more consistent with the construction process of concrete. For this reason, the author firstly fabricated a shear box test apparatus, as shown in Fig. 1, which can increase or decrease shear stress through a shear rate control or a shear stress control [32,50]. During the rate-controlled stress growth test, the bottom of the two rotating plates of the shear box are fixed. The tops of the rotating plates are driven by a

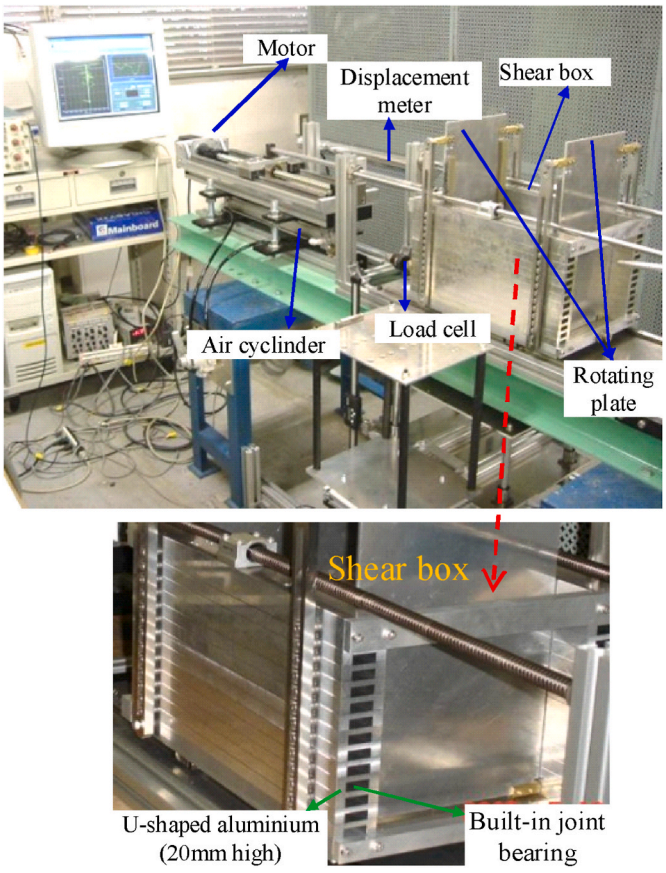

Fig. 1. Shear box test apparatus [32,50].

motor. In case of the stress-controlled stress growth test, the tops of the rotating plates are fixed, but the bottoms are pushed by an air cylinder. The front and rear walls of the shear box are constructed of U-shaped aluminum parts connected by linear bearings embedded inside them. Fresh concrete samples were packed in a soft plastic bag, and then placed into the shear box. The resistance of the device and the plastic bag was evaluated beforehand using the reference material [45]. The τ–γ, $\dot{\gamma}$ relationships of cement paste, mortar and fresh concrete were measured in detail by the two stress growth methods [32,50]. The effects of normal stress, fluidity of fresh concrete, loading speed in case of the stress-controlled test, sample's thickness, shearing time, and volume concentration of solid particles on the τ–γ, $\dot{\gamma}$ relationships were also investigated. Fig. 2 shows some experimental results of the τ–γ, $\dot{\gamma}$ relationships [32]. The shear strain increases with the shear stress, but the τ–γ relational curve can be divided into three parts: first rapid increase stage, slow increase stage and secondary rapid increase stage. Also, the τ–$\dot{\gamma}$ relational curves can be divided into three parts: first increase stage, decrease stage and secondary increase stage.

Since the maximum shear strain available for the shear box test is limited, the τ–γ, $\dot{\gamma}$ relational curves of the mortars and the concretes exhibited only two stages in Fig. 2. For measuring the whole τ–γ, $\dot{\gamma}$ relational curves of fresh concrete from shear deformation before yielding to shear flow after yielding, the author further produced a parallel plate rheometer like BTRHEOM, as shown in Fig. 3 [51]. An air motor drives the lower rotating blade, thus the measurement can be conducted by a stress-controlled stress growth method. The distance between the upper and lower blades can be set arbitrarily in the range of 250 mm. In our past fresh mortar experiments and fresh concrete experiments, the maximum sizes of fine and coarse aggregates used were 5 mm and 20 mm, respectively, and the distance was set to 50 mm and 100 mm respectively. Using this rheometer, the whole flow curves of fresh concretes and fresh mortars were measured. The measurement results of fresh mortars are shown in Fig. 4 [51], where the three stages of shear strain and shear rate changes can be clearly identified. In the secondary rapid increase stage, the shear strain increases but the shear

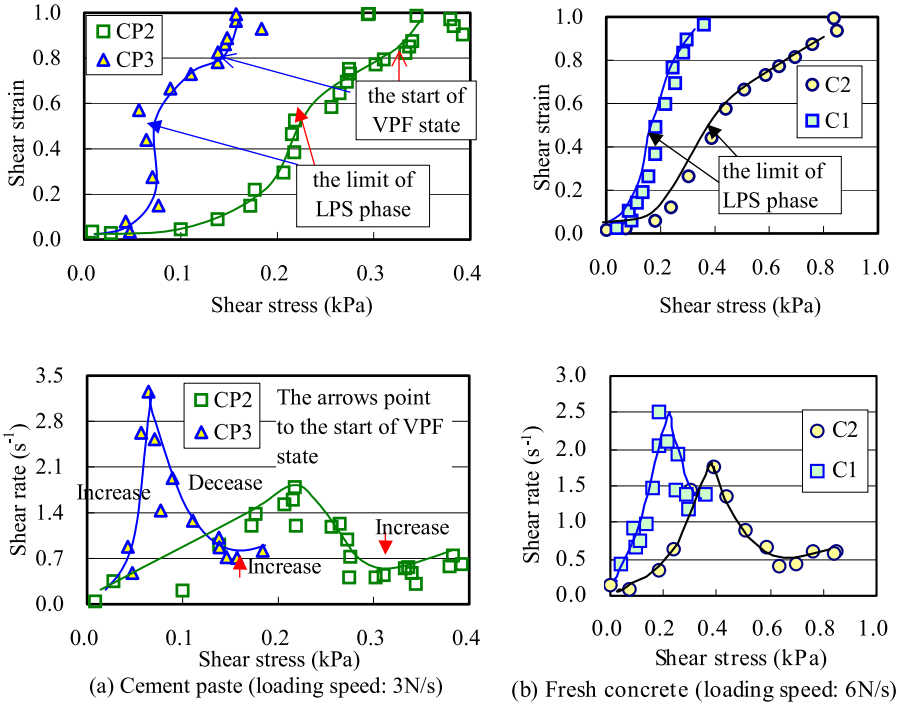

Fig. 2. The shear stain, shear rate-shear stress relationships of fresh cement paste (CP) and fresh concrete (C), measured by the stress-controlled stress growth test of shear box (fluidity: CP3 > CP2, C1 > C2, LPS phase and VPF state refer to the loose particle structure phase, and the viscoplastic flow state, respectively, as detailed in Fig. 6) [32].

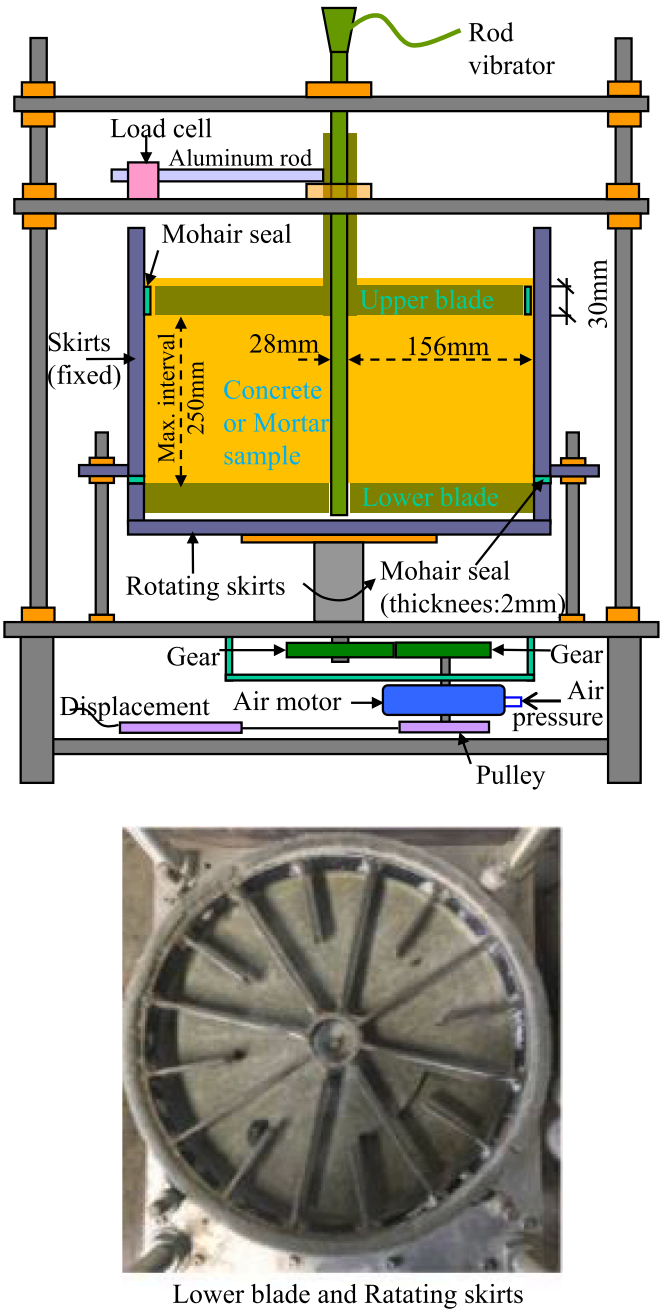

Fig. 3. Stress-controlled parallel plate rheometer [51].

stress decreases, and the shear rate rapidly increases with the increase of shear stress. The fresh concretes also exhibited the same trends as in Fig. 4, though their results are not shown here.

Fig. 5 shows the effects of external vertical pressure and loading speed on the τ–γ, $\dot{\gamma}$ relationships, measured by the stress-controlled stress growth test of the shear box [32]. The external vertical pressure was applied during shearing, and pre-shearing prior to the measurement was not conducted. As shown in Fig. 5, with the increase of external vertical pressure or the decrease of loading speed, the peak shear rate of the τ–$\dot{\gamma}$ relational curve decreases, while the shear stress corresponding to the peak shear rate increases.

Roussel et al. [33] interpreted that the rapid increase (linear stress growth) phase of τ–γ relational curve of cement paste before yielding is associated with a very stiff elastic behavior at low strain, caused by the chemical links (C–S–H gel bridges) between cement particles. However, for fresh concrete or fresh mortar, the interactions of solid particles are more complicated than cement paste, there are large inter-friction and inter-locking (jamming) between aggregate particles, not just the chemical bonds of hydrates. Therefore, the occurrence of pure elastic behavior is questionable for fresh mortar or concrete. Not only the amount of particle contact points, but also the locations of the particle contact points affect the resistance to particle movement because solid particles have different sizes, shapes and surface textures. At the beginning of load, the particles are randomly distributed, and the particles are in contact only to support their gravity in order to maintain the initial material shape. Hence, the particles do not need to be in close contact with each other, resulting in a loose particle configuration. The author believes that the first rapid increase of γ, $\dot{\gamma}$ with τ is due to the initial loose particle structure, which makes particle motion and material deformation easy in the early small deformation period. Here, the first rapid increase stage of the γ, $\dot{\gamma}$–τ relational curves is called as Loose Particle Structure (LPS) phase. However, as shear stress increases, the particles have to contact closely with neighboring particles to support the increasing shear stress [52,53]. Close particle contact would certainly cause the difficulty in migration of particles and the great resistance to migration. The particle configuration becomes closer and closer as shear deformation increases. Thus, after a certain shear deformation (critical shear strain of LPS phase), the shear strain increases slowly, i.e. well-known strain hardening behavior of material, accordingly the shear strain rate decreases with increasing shear stress. Here, the slow increase of shear strain and the decrease of shear strain rate with shear stress are considered as the behaviors in Close Particle Structure (CPS) phase. The shear stress, which occurs at the transition from the LPS phase to the CPS phase, is defined as LPS limit stress here.

However, there is a limit to increasing the tightness of particle contacts, thus the particle contacts are not further tightened at high shear stresses, conversely the flocculated particle structure is broken, resulting in shear thinning and the secondary rapid increase in shear strain and shear rate. In the mechanics of granular materials such as soil and sand, this stage is generally referred to as the shear failure state. Here, it is called viscoplastic flow state of fresh concrete. The maximum shear stress in the CPS phase is defined as the static yield stress, at which the shear rate is very small or even close to zero, and fresh concrete behaves from solid-like viscoelastic deformation (VED) to liquid-like viscoplastic flow (VPF). Based on the above experimental results, the author summarized the viscoelastic deformation behavior and the viscoplastic flow behavior, as shown in Fig. 6 [32,51]. Depending on the fluidity of material, and the normal stress, etc., the first rapid increase stage and the slow increase stage of shear strain have different ranges, and the $\dot{\gamma}$–τ relationship in the LPS phase is linear or non-linear. Mishima et al. [54] also observed the viscoelastic deformation behavior at a shear strain range of 0–1.2 for fresh mortar by the shear rate-controlled stress growth test using a vertical type shear box rheometer (the shear plane is vertical).

In the VED state, fresh concrete shows the solid-like behavior, whereas in the VPF state, it exhibits the liquid-like behavior. Fig. 7 shows a comparison of the rheological behaviors measured for the same fresh concrete by the stress-controlled stress growth method, and the shear rate growth method, respectively [50]. Obviously, the shear rate growth method cannot measure the viscoelastic deformation behavior before yielding, but it is applied to the measurement of the viscoplastic flow behavior after yielding.

3. Development of microscopic approach to rheological behaviors

3.1. Constituent model

Fresh concrete is a kind of granular fluid or viscous particle assembly, consisting of binder particles, aggregate particles and water. Between binder particles with surface charges, in addition to the van der Waals attraction, there are electrostatic repulsive and steric forces from

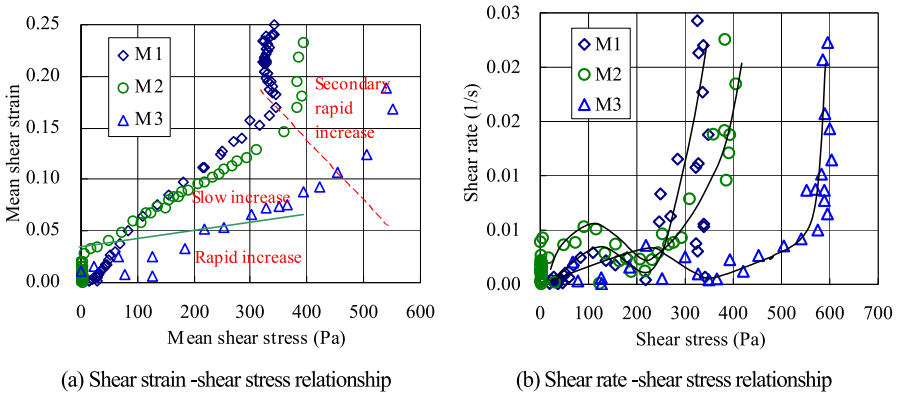

(a) Shear strain -shear stress relationship (b) Shear rate -shear stress relationship

Fig. 4. Shear deformation and flow of fresh mortar (M), measured by the stress-controlled stress growth test of the parallel plate rheometer (Fluidity: M1 > M2 > M3) [51].

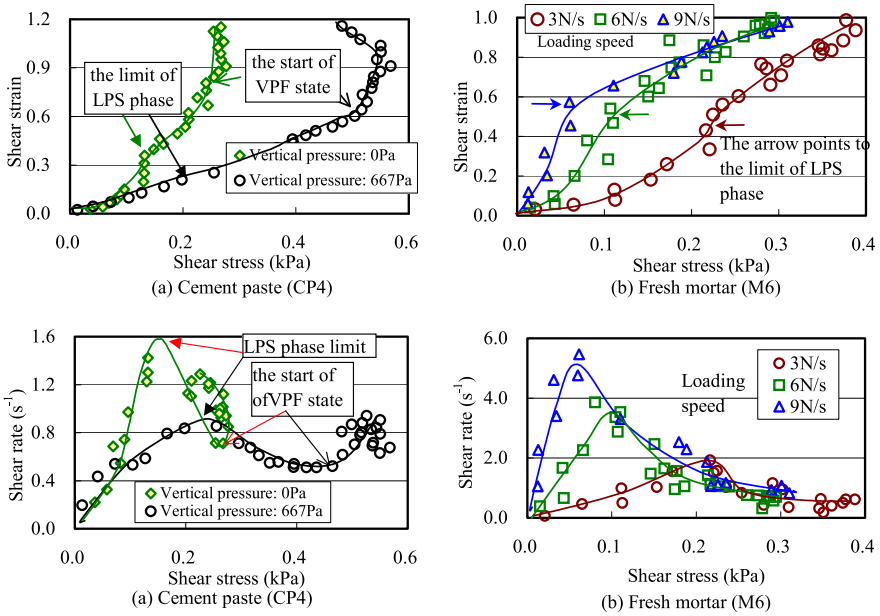

Fig. 5. Effects of vertical pressure and loading speed on the shear stain and shear rate of fresh cement –based materials (LPS phase and VPF state refer to the loose particle structure phase, and the viscoplastic flow state, respectively, as detailed in Fig. 6) [32].

species (especially polymers) adsorbed on the binder particle surfaces. These forces form a potential energy that affects particle migration, flocculation and dispersion. As a result, fresh cement paste exhibits a time-dependent deformation behavior under stress or load. In contrast, the displacement of aggregate particles is time-independent since they have no potential energy, and instantaneous deformation occurs once aggregate particle is subjected to a force. Thus, both instantaneous and time-dependent particle migrations occur when fresh concrete is sheared, which has already been confirmed by the experiments using the shear box apparatus [55]. Therefore, solid particles in fresh concrete can be classified into two types: viscous particles - binder particles whose displacement increases with time, and non-viscous particles - aggregate particles whose displacement is time-independent. The resistance resulted from the potential energy is considered as viscous resistance because it occurs only when the balance of the above-mentioned forces acting on binder particles is broken, and the binder particles are displaced. As explained before, it is impossible to have no particle contact in fresh cement-based materials. There should be interparticle friction due to the particle contact, and the frictional resistance follows the Coulomb's law of friction. The interparticle friction angle depends on the texture and wetness of particle, and is distinguished into static and dynamic friction angles. When fresh concrete deforms, moving particles are present, but there are still standing particles, thus the average friction angle varies with the ratio of the moving and standing particles. In this study, for convenience, the static and dynamic frictional angles are not distinguished, assuming that average interparticle friction angle is a constant for a certain fresh concrete.

Mixing water is absorbed on the surface of solid particles or exists in the interparticle pores. The surface tension of unsaturated pore water causes a capillary pressure, called cohesion, which increases internal friction of fresh concrete [26]. By the way, when fresh concrete is subjected to shear force or vibration, an excess pore water pressure would occur, which causes bleeding [56]. If the particles in fresh concrete are considered as spheres, the average value (f_{wm}) of capillary pressures (f_w) is expressed by Eq. (3.1) [25].

$$f_{wm} = \frac{2\pi r_m \Gamma}{1 + \tan(\varphi_m/2)} \tag{3.1}$$

where, f_{wm} is average capillary pressure caused by pore water, Γ is surface tension of pore water, φ_m is average contact angle between solid

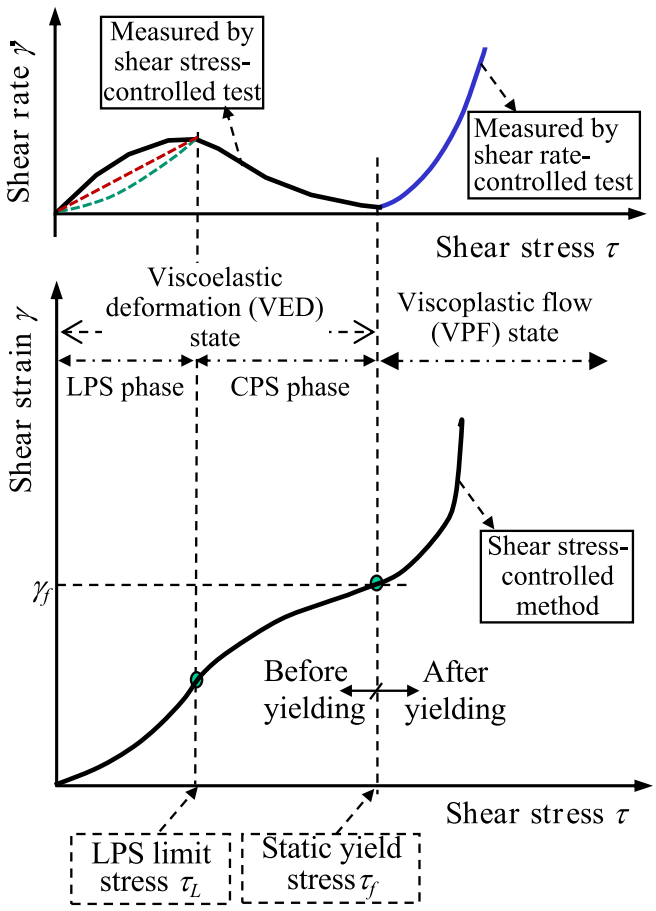

Fig. 6. Conceptual illustrations of the $\dot{\gamma}$, $\gamma-\tau$ relationships based on the experimental results [32,51].

and water, and r_m is average radius of particles.

Solid particles transfer their interparticle forces, rising from their own weight and external force, to neighboring particles through particle contact points. The contact plane of two particles is at a certain angle to the plane of maximum shear stress (abbreviated as MS plane), as shown in Fig. 8 [12]. This angle is referred to as particle contact angle (PCA). Particle configuration of granular material is generally described by the distribution and median of PCA [46]. The author found that the PCA of fresh mortar is in a normal distribution by X-ray imaging [52,57]. Due to the PCA, the particle is subject to a resistance when sliding over neighboring particles, and dilatancy happens along with the shear deformation in granular material [42,46,53]. The resistance to particle migration by PCA is referred to here as dilatancy resistance.

It is generally considered that the thixotropy of fresh cement-based materials is attributed to the flocculation/de-flocculation of particles. However, there is no indicator to express quantitatively the degree of particle flocculation. To deal with the granular feature of fresh cement-based materials, the PCA is introduced in this study to reflect the tightness of particle configuration. Therefore, solid particles are subjected to the frictional resistance (τ_ϕ) caused by the interparticle frictional angle (ϕ), the dilatancy resistance (τ_θ) caused by the PCA, and the cohesion resistance (τ_w) caused by the capillary pressure of pore water. Besides the three resistances, the binder particles also meet the viscous resistance (τ_v) due to the potential energy. Based on the above discussion, the multiphase model of fresh concrete is proposed, as shown in Table 1.

Due to small dosage, chemical admixture, e.g. water reducing agent (WRA), is not considered as a separate phase here. The WRA addition increases the dispersion of binder particles and the fluidity of fresh concrete. These effects of WRA are reflected through the rheological model parameters explained later, e.g. average potential energy of binder particles (E), average value (θ) of PCA, and average interparticle frictional angle (ϕ), etc.

3.2. Particle migration behavior

Once the interparticle force, exposed to an aggregate particle, surpasses the sum of $\tau^* = \tau_\phi+\tau_\theta+\tau_w$, the aggregate particle will become a moving particle. However, for a binder particle, it will not yet move unless the viscous resistance τ_v is also overcome. The binder particles whose interparticle forces surpass only the τ^* are called active binder particles. The probability of occurrence of moving aggregate particles or active binder particles is expressed by Eq. (3.2) [46].

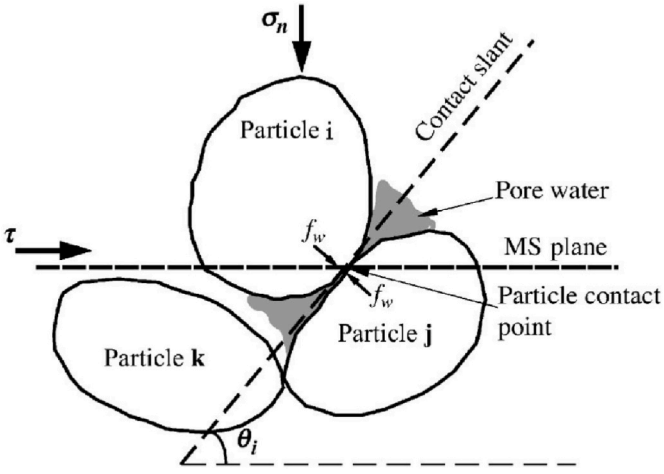

Fig. 8. Particle contact point and particle contact angle (θ_i is PCA, σ_n represents normal stress) [12].

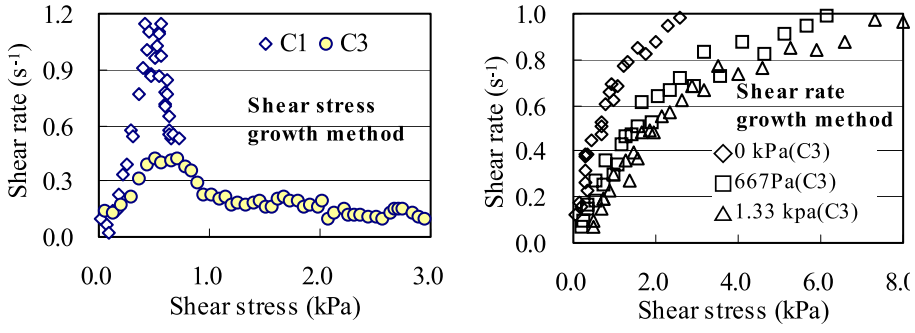

Fig. 7. Effects of test methods on the shear rate –shear stress of fresh concrete (C)(fluidity: C1 > C3) [50].

Table 1
Multiphase model of fresh concrete.

Component	Feature	Exposed resistance, etc.		Displacement
		At rest	Moving state	
Binder particle	Viscous	• Static friction • Dilatancy resistance • Cohesion resistance	• Dynamic friction • Dilatancy resistance • Viscous resistance • Cohesion resistance	Time-dependent
Aggregate particle	Non-viscous		• Dynamic friction • Dilatancy resistance • Cohesion resistance	Time-independent
Water	Fluid	• Surface tension and suction cause capillary pressure to particles		–

$$P=\frac{1}{\sqrt{2\pi}\cdot\rho}\int_{-\infty}^{m_1}\exp\left[-\frac{(m_1-m_2)^2}{2\rho^2}\right]dm_1 \tag{3.2}$$

where, P is probability of moving aggregate particles or active binder particles, ρ is standard deviation, m_1 is average directional angle (β) of interparticle forces, and m_2 is equal to $\theta+\phi$.

However, as shown in the $P\sim m_1$ curves of Fig. 9(a), the β_i and ($\theta_i+\phi_i$) exhibit approximately normal distributions. It is unreasonable that the distribution range of the P extends to infinity on two sides, as shown in Fig. 9(b). Therefore, for convenience of calculation, a linear function P_t shown in Eq. (3.3) is used as an approximate expression of the P to avoid this problem [46]. When m_1 is equal to zero and m_2, the values of P_t are 0 and 0.5, respectively (see Fig. 9(c)).

$$P_t=m_1/2m_2,\quad m_2=\theta+\phi \tag{3.3}$$

The tangent of the expected value m_1 ($=\beta$) of the directional angles of interparticle forces is equal to a ratio of shear stress to normal stress (σ_n)

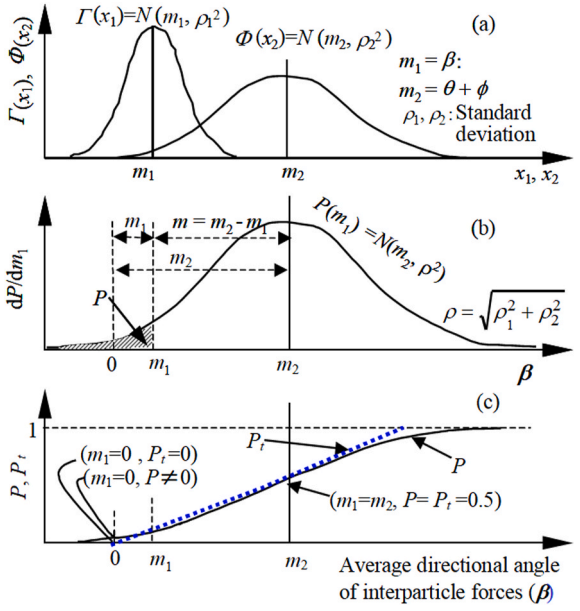

Fig. 9. Probability of occurrence of moving aggregate particles or active binder particles [46]: (a) Distributions of the directional angles of interparticle forces (β_i), and the motion resistance angles ($\theta_i+\phi_i$) of particles. (b) Variation of the P with the β ($=m_1$). (c) Approximation of the P with the linear function P_t.

on the MS plane, as shown in Eq. (3.4) [46]. The force acting on fresh concrete is generally a compression, e.g. gravity and pumping pressure, and the maximum resulting shear stress is less than the normal stress on the MS plane according to the Mohr's stress circle. Therefore, tanm_1 is generally less than 1.0, and the approximation of Eq. (3.4) is valid.

$$m_1\approx\tan m_1=\frac{\tau}{\sigma_n+N^*f_{wm}\cos\theta} \tag{3.4}$$

where, σ_n is normal stress on the MS plane caused by external force and self-gravity, and N^* is number of particle contact points on per unit area of the MS plane.

It is assumed that a particle has only one contact point with other particles on the MS plane. If there are multiple contact points, the points are combined into one. Thus, the number of particle contact points on the MS-plane is equal to the number of particles ($N^*=N$).

Substituting Eq. (3.4) into Eq. (3.3), the probability of occurrence of moving aggregate particles or active binder particles is expressed by Eq. (3.5)

$$P_t\approx\frac{\tau}{2(\sigma_n+Nf_{wm}\cos\theta)(\theta+\phi)} \tag{3.5}$$

Wallevik [40] reported that the shear thinning of fresh concrete is not only due to thixotropic behavior of cement paste, but also related to continuous aggregate particle migration. According to the Murayama's theory of particle assembly [46], some particles have to move to contact closely with neighboring particles to support the increasing shear stress, thus the particle configuration becomes tighter and tighter as shear stress increases in the viscoelastic state, as mentioned earlier. The greater the shear stress, the greater the average PCA of particle assembly. However, since there is a limit to the increase in the particle contact tightness, once the shear stress exceeds the static yield stress, fresh concrete enters into the viscoplastic flow state, where some of the particles cannot reach stable positions to support their subjected interparticle forces, and thus keep moving in theory if there is no boundary obstruction. Such particles are called failure particle. As the PCA of failure particle decreases with its movement, the interparticle force supported by the failure particle decreases. The interparticle force portion unsupported by the failure particle has to be burdened by the adjacent moving or static particles. Therefore, once a failure particle is generated, other failure particles around it occur acceleratedly, the particle configuration tightened in the viscoelastic state becomes looser and looser, thus the average PCA decreases with the increase of failure particles, and gradually approaches to zero. When the θ becomes zero, fresh concrete enters into a residual state like other granular materials such as soil and sand. Fig. 10 shows the variation of particle contact and average PCA with shear deformation from the initial state to the viscoplastic flow state.

The author investigated the relationships between the average PCA (θ) and the shear stress or shear displacement by X-ray CT imaging of fresh mortar [52], and the intern-visualized experiments (Laser - Aided Tomography, LAT) of two simulated fresh concretes that were mixtures of silicon oil and round glass particles or randomly-shaped glass particles [53]. As shown in Fig. 11, because the silicon oil and the glass particles had the same refractive index, the contours of glass particles and particle contact points could be seen under the green laser light irradiation. One side shear test was performed for the simulated concretes, the shear deformation under different shear stresses was recorded, and the dilatancy phenomenon along with the shear deformation was also observed. The particle contours under different shear deformations were photographed, and then the angles, i.e. PCA, formed by the particle contact planes and the shear plane (horizontal plane) were measured. The description of the intern-visualized experiments can also be found in Ref. [57]. Some of the LAT experimental results are shown in Fig. 12. The average PCA (θ) of granular fluid increases with increasing shear displacement, but gradually decreases after reaching a peak value. According to the results shown in Fig. 12(e), the $\theta-\tau$ relationship in the

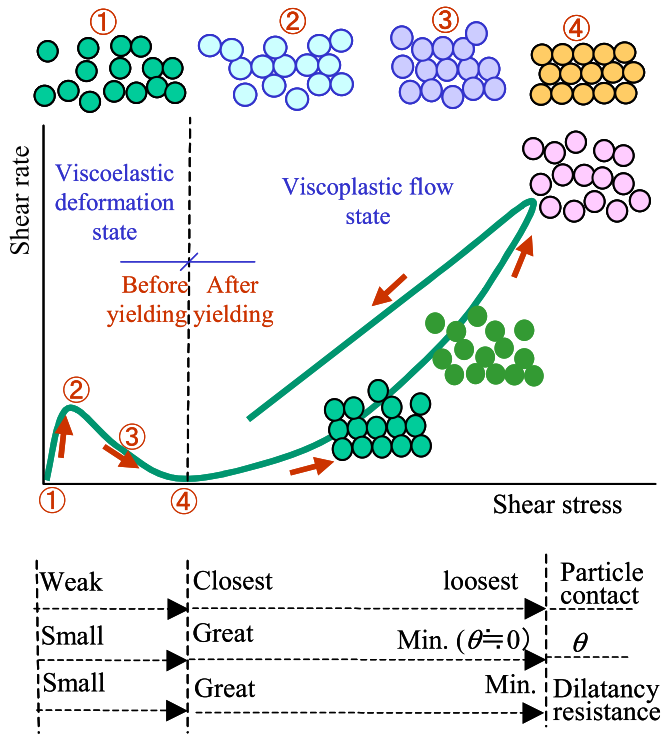

Fig. 10. Changes of particle contact angle and dilatancy resistance with shear deformation or flow.

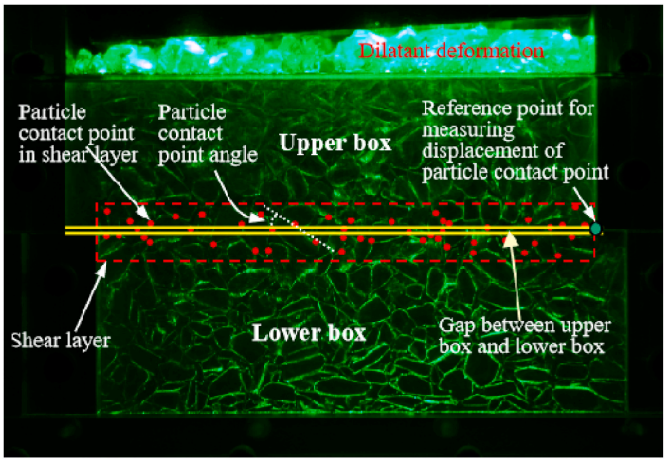

Fig. 11. Internal visualization of the simulated fresh concrete in one-sided shear test [53].

viscoelastic deformation state is expressed by the first equation of Eq. (3.6). This equation only indicates the ultimate average PCA resulting from a shear stress, ignoring the variation of θ with the elapsed time before reaching the ultimate θ value because the material has a small displacement before yielding, i.e. the elapsed time before reaching the ultimate θ value is very short.

It is reported that due to the structural breakdown of cement paste, the torque (T_q) of rotational rheometer decreases with time t at a constant shear rate from the initial value T_{q0} to the equilibrium value T_{qE}, and the exponential function ($T_q = T_{qE} + (T_{q0} - T_{qE})\exp(-Bt)$) is suitable to express the T_q - t relationship of cement paste, in which the parameter B increases with the shear rate [17]. In this study, referring this finding and based on the LAT experimental results shown in Fig.12 (a) ~ (d), the $\theta - \gamma$ relationship in the viscoplastic flow state was proposed as shown in the second equation of Eq. (3.6).

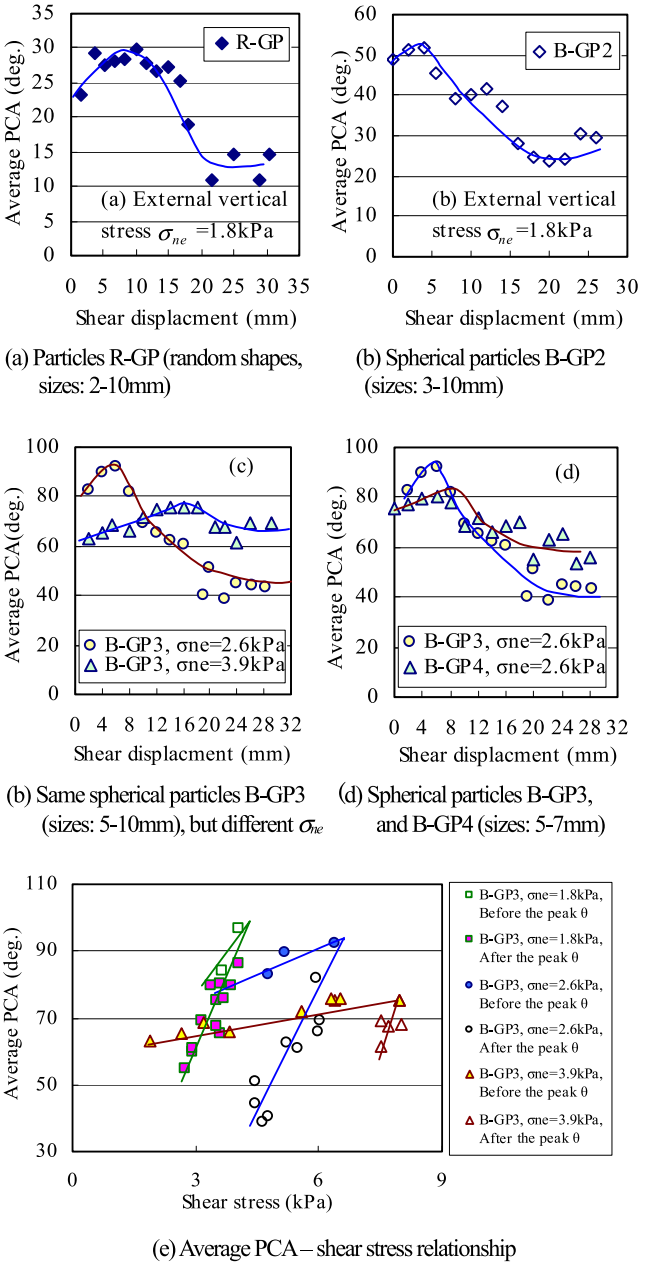

(a) Particles R-GP (random shapes, sizes: 2-10mm)

(b) Spherical particles B-GP2 (sizes: 3-10mm)

(b) Same spherical particles B-GP3 (sizes: 5-10mm), but different σ_{ne}

(d) Spherical particles B-GP3, and B-GP4 (sizes: 5-7mm)

(e) Average PCA – shear stress relationship

Fig. 12. Relationships between average PCA (θ) and shear displacement, shear stress [53].

Viscoelastic deformation state:

$$\theta = \theta_0 + \frac{\theta_f - \theta_0}{\tau_f}\tau$$

Viscoplastic flow state:

$$\theta = \theta_f \exp(-\kappa \cdot \gamma_i) \tag{3.6}$$

$$\gamma_i = \begin{cases} \dot{\gamma} \cdot t & \text{single shear rate } \dot{\gamma} \text{ sustained} \\ \gamma_{i-1} + \dfrac{\dot{\gamma}_{i+1} - \dot{\gamma}_i}{s_2}\dot{\gamma}_i & \text{shear rate gowth at speed } s_2 \\ & (i = 1, 2, \ldots, n) \end{cases}$$

where, t is duration of shear rate $\dot{\gamma}$ or the elapsed time to reach the $\dot{\gamma}$, θ_0 and θ_f are initial average PCA of fresh concrete before sheared, and the average PCA at yielding point, respectively, θ_{f0} is average PCA at the beginning of the viscoplastic flow state, and $\theta_{f0} = \theta_f$ in the case of

continuous loading from the VED state to the VPF state, κ is proportional coefficient, and γ_i represents total shear strain in time t.

3.3. Shear resistance caused by granular characteristic

The shear resistance τ^* ($=\tau_\phi+\tau_\theta+\tau_w$), induced by granular characteristic of fresh concrete, is expressed by Eq. (3.7) [12]. Though the C_{w1} varies with the value of θ, treating the C_{w1} as a constant here for a given concrete does not lead to a large difference since the C_{w1} is small.

$$\tau^* = \sigma_n \tan(\theta+\phi) + C_{w1} \tag{3.7}$$

$$C_{w1} = \frac{Nf_{wm}}{\cos\theta(1-\tan\theta\tan\phi)}$$

Faroug et al. [26] suggested that the internal friction is related to the effective normal stress that is a difference between normal stress and neutral hydrostatic pressure of pore water. In fact, the pore water pressure depends on the strength of granular structure, and the prediction of the pore water pressure is not easy. A strong particle structure, i.e. having a large θ, has a large frictional resistance, as shown in Eq. (3.7). The pore water pressure is resulted from the interparticle force portion that cannot be supported by the particle structure [56]. For a strong particle structure with a large average PCA, the pore water pressure is small so that the effective normal stress is large. Hence, it is not necessary to consider the pore water pressure since the average PCA was introduced in this study.

3.4. Relationship between shear deformation and particle migration

The suspension behavior is explained as a consequence of stress-driven particle migration. As a dense suspension, the deformation of fresh concrete is essentially caused by the particles migration. Eyring's rate process theory explains that matter deformation is resulted from the movement of flow units under external force, and only the constituent units of matter that overcome the potential energy barrier to motion will become the flow units [46]. Because the binder particles have potential energy and are subjected to the non-viscous resistance τ^*, the author extended the Eyring's theory to express the probability of occurrence (P_c) of moving binder particles on per unit area of the MS plane in per unit time by Eq. (3.8) [12].

$$P_c = 2A\sinh\left(\frac{\tau_v\cdot\Lambda_c}{2kT\cdot N_c\cdot P_t\cdot L_0^{-2}}\right)$$

$$A = \frac{kT}{h}\exp\left(-\frac{E}{kT}\right) \tag{3.8}$$

where, E is average potential energy of binder particles, T is absolute temperature, Λ_c is average displacement of moving binder particles till they reach new stable positions, τ_v is shear stress portion exposed to binder particles to overcome the viscous resistance ($=\tau-\tau^*$), k is Boltzmann's constant (1.380662×10^{-23} J/k), h is Planck constant (6.626×10^{-27} erg • s), N_c is number of binder particles on per unit area, P_{tc} is the probability of occurrence of active binder particles, and L_0 is unit length (=1.0).

The author also applied the Murayama's particle assembly theory [46] to fresh concrete to obtain the shear strain equation for fresh concrete, as shown in Eq. (3.9) [12].

$$\gamma = n\cdot\Lambda\cdot\cos\theta/L_0 \tag{3.9}$$

where, n is number of moving particles on per unit area of the MS-plane, and Λ is average displacement of moving binder particles and moving aggregate particles.

At present, there is no method to investigate the average displacement (Λ) of moving particles, and relevant study has not been found. Before yielding, some particles must move to new stable positions with larger PCAs than their previous positions to support their imposed external force. Particles with larger PCAs generally need to travel longer distances to reach new locations with much larger PCAs. Hence, it is assumed that the larger the θ, the larger the Λ of moving particles. In this study, the change of Λ in the VED state is approximately expressed by the first equation of Eq. (3.10).

In the viscoplastic flow state, the failure particle is not able to reach new stable position in theory since it is exposed to a large interparticle force, so that it will continue to move without stopping if there is no boundary obstacle. However, in fact the failure particle should either be stopped by stationary particles or move together with adjacent non-failure moving particles. Therefore, the average travel distance of failure particles is probabilistically the same as that of non-failure moving particles. It is reasonable to assume that average displacement of failure particles and non-failure moving particles is equal to the maximum average displacement of the moving particles before yielding, i.e. in the CPS phase of VED state. The Λ in the viscoplastic flow state is expressed by the second equation of Eq. (3.10) according to the first equation in Eq. (3.10).

$$\textit{Viscoplastic deformation state}: \ \Lambda = \Lambda_0/\cos\theta$$

$$\textit{Viscoplastic flow state}: \ \Lambda = \Lambda_0/\cos\theta_f \tag{3.10}$$

where, Λ_0 is average displacement of moving particles in the beginning of the viscoelastic deformation state.

By combining Eqs. (3.8) and (3.9), the shear strain caused by the movement of binder particles in unit time, i.e. shear strain rate, was obtained, as shown in Eq. (3.11). For simply expressing the subsequent equations, the L_0 (=1.0, dimension: m) was omitted in the subsequent equations.

$$\dot\gamma = P_c\cdot P_{tc}\cdot N_c\cdot\Lambda\cdot\cos\theta/L_0 \tag{3.11}$$

4. Theoretical analysis of shear deformation and flow models

4.1. Viscoelastic deformation model before yielding

The shear strain of fresh concrete is expressed by Eq. (4.1). The derivation process can be found in Appendix.

$$\gamma = \frac{c_6\cdot\tau/(\sigma_n+C_{w2})}{c_2+c_3\tau}[1-\exp(-qt)]$$

$$c_6 = \frac{1}{2}\frac{N\Lambda_0}{L_0} \tag{4.1}$$

According to Eq. (4.1), the shear strain resulting from a constant shear stress increases from zero with time t, and eventually approaches to a maximum value, as shown in Eq. (4.2).

$$(\gamma)_{t=0}=0, \ \ (\gamma)_{t\to\infty} = \frac{c_6\cdot\tau/(\sigma_n+C_{w2})}{c_2+c_3\tau} \tag{4.2}$$

The shear strain rate can be obtained as Eq. (4.3) by differentiating Eq. (4.1) for time t.

$$\dot\gamma = c_7\cdot\tau(c_2+c_3\tau)\exp(-qt)$$

$$c_7 = \frac{\Lambda_0\Lambda_c L_0}{h(\phi+\theta_0)\exp(E/kT)} \tag{4.3}$$

Eq. (4.1) shows that the shear strain increases with increasing shear stress or decreasing normal stress. The derivation of shear rate with respect to shear stress is shown in Eq. (4.4). Eq. (4.4) indicates that the shear rate has a maximum in the viscoelastic deformation state. The shear stress corresponding to the peak shear rate is the LPS limit stress, as described earlier. That is, according to Eq. (4.3), the shear rate first increases, then decreases with increasing shear stress. By letting $d\gamma/d\tau=0$, the LPS limit stress can be obtained from Eq. (4.4), and then the

peak shear rate can also be obtained by substituting the LPS limit stress into Eq. (4.3). But since these expressions are very complicated, they are omitted here.

$$\frac{d\dot{\gamma}}{d\tau} = c_7[c_2 + 2c_3\tau(1-q)]\exp(-qt) \tag{4.4}$$

According to Eq. (4.1), the duration (t_f) of shear stress till yielding can be expressed by Eq. (4.5).

$$t_f \approx \frac{\gamma_f h(\phi+\theta_0)\exp(E/kT)}{\tau_f(\phi+\theta_f)\Lambda_0\Lambda_c} \tag{4.5}$$

Combining Eqs. (4.3) and (4.5), the shear rate (γ_f) at the yielding point is expressed by Eq. (4.6). γ_f increases with the increase of τ_f or the decrease of σ_n, but γ_f is extremely small because the c_7 is small.

$$\dot{\gamma}_f = c_7\tau_f(\phi+\theta_f)\exp\left(-\frac{2\gamma_f(\phi+\theta_f)(\sigma_n+C_{w2})}{N\Lambda_0\tau_f}\right) \tag{4.6}$$

The shear resistance in the viscoelastic deformation state can be expressed in form of Kelvin-Voigt model, as shown in Eq. (4.7), by combining Eq. (A.7) of Appendix, Eq. (4.1), and Eq. (4.3).

$$\tau = G\gamma + \eta_b\dot{\gamma},$$

$$G = \frac{c_2}{c_6/(\sigma_n+C_{w2})}\cdot\frac{c_2+c_3\tau}{c_2+c_3\tau\exp(-qt)},$$

$$\eta_b = \frac{1}{c_7}\cdot\frac{1}{c_2+c_3\tau\exp(-qt)} \tag{4.7}$$

On the other hand, in the stress-controlled stress growth test method with a loading speed (s_1), using Eq. (4.1), the shear strain can be expressed by Eq. (4.8). After substituting $\tau = s_1\cdot t$ into Eq. (4.1), and differentiating with respect to the elapsed time t, the shear rate equation can be obtained, as shown in Eq. (4.9).

$$\gamma_i = \gamma_{i-1} + \frac{c_6\cdot\tau_i/(\sigma_n+C_{w2})}{c_2+c_3\tau_i}\left[1-\exp\left(-q\frac{\tau_{i+1}-\tau_i}{s_1}\right)\right] \qquad (i=1,\ 2,\ \cdots,n) \tag{4.8}$$

$$\dot{\gamma} = \frac{c_2c_6s_1/(\sigma_n+C_{w2})}{(c_2+c_3\tau)^2}\left[1-\exp\left(-q\frac{\tau}{s_1}\right)\right] + \frac{c_7\tau(c_2+3c_3\tau)}{\exp(q\tau/s_1)} \tag{4.9}$$

4.2. Viscoplastic flow model after yielding

After yielding, fresh concrete enters the viscoplastic flow state, the shear resistance $\tau^*_f(=\tau_\phi+\tau_\theta+\tau_w)$ induced by the granular characteristics of fresh concrete is expressed by Eq. (4.10), based on the second equation of Eq. (3.6) and Eq. (3.7). At the yielding point, the shear strain of viscoplastic flow is zero, i.e. $\gamma_i = 0$, thus the static yield stress τ_f is expressed by Eq. (4.11).

$$\tau^*_f = \sigma_n\tan(\theta_f e^{-\kappa\cdot\gamma_i}+\phi) + C_{w1} \tag{4.10}$$

$$\tau_f = \sigma_n\tan(\theta_f+\phi) + C_{w1} \tag{4.11}$$

Therefore, the shear stress portion τ_v is shown in Eq. (4.12), which is used to overcome the viscous resistance of moving binder particles in the viscoplastic flow state.

$$\tau_v = \tau - \tau^*_f \tag{4.12}$$

Combining the Eq. (3.8), the second equation of Eq. (3.10), and Eq. (3.11), the shear rate after yielding can be calculated by Eq. (4.13)

$$\dot{\gamma} = 2A\sinh\left(\frac{\Lambda_c}{2kT}\cdot\frac{\tau-\tau^*_f}{P_{tc}N_c}\right)P_{tc}N_c\frac{\Lambda_0}{\cos\theta_f}\cos\theta \tag{4.13}$$

The number (N_c) of binder particles is generally large (especially in high fluidity concrete or mortar with large cement content). Thus, the value of $\Lambda_c\ (\tau-\tau^*_f)/(2\ k\ T\ P_{tc}\ N_c)$ in Eq. (4.13) is small. The approximate equation of shear rate is shown in Eq. (4.14) since $\sinh x \fallingdotseq x$ is valid when x is small.

$$\begin{aligned}\dot{\gamma} &\approx 2A\left(\frac{\Lambda_c}{2kT}\cdot\frac{\tau-\tau^*_f}{P_{tc}N_c}\right)P_{tc}N_c\frac{\Lambda_0}{\cos\theta_f}\cos\theta \\ &= \frac{A\Lambda_c\Lambda_0}{kT}\cdot\frac{\cos\theta}{\cos\theta_f}\cdot\left(\tau-\tau^*_f\right)\end{aligned} \tag{4.14}$$

Substituting the second equation of Eq. (3.6) and Eq. (4.12) into Eq. (4.14), the shear resistance of fresh concrete after yielding can be obtained, as shown in Eq. (4.15).

$$\begin{aligned}\tau &= \left[\sigma_n\tan(\theta_f e^{-\kappa\cdot\gamma_i}+\phi)+C_{w1}\right] + \frac{\eta}{\cos(\theta_f e^{-\kappa\cdot\gamma_i})}\dot{\gamma} \\ &= \tau^*_f + \eta_a\dot{\gamma} \qquad (\tau>\tau_f,\ \gamma>\gamma_f,\ t>t_f) \\ \eta &= \frac{\cos\theta_f h\exp(E/kT)}{\Lambda_0\Lambda_c},\ \eta_a = \frac{\eta}{\cos(\theta_f e^{-\kappa\cdot\gamma_i})}\end{aligned} \tag{4.15}$$

where, τ^*_f, η_a are called apparent yield stress, and apparent plastic viscosity, respectively, η is a constant for a given concrete, called basic viscosity here, but depending on environmental temperature, and γ_i represents the shear strain of viscoplastic flow at time t (see Eq. (3.6)).

In case of the rate-controlled stress growth test without the viscoelastic deformation stage, the θ_f in Eq. (4.15) should be equal to θ_0, but the θ_f in the basic viscosity η remains the same.

As shown in Eq. (4.10), the apparent yield stress τ_f*, resulting from the granular characteristics, decreases with shear flow (the value of γ_i) but increases with increasing σ_n. The apparent viscosity η_a decreases with the advance of shear flow, and eventually approaches to the basic viscosity η. That is to say, the η_a decreases with increasing the shear rate and the elapsed time. Therefore, Eq. (4.15) can describe the shear thinning behavior of fresh concrete after yielding. It should be noted that Eq. (4.15) can not describe the shear thickening behavior caused by the cement hydration in long-term rheological experiment.

If the effect of stress duration on the shear resistance is not considered (i.e. $t=0\rightarrow\gamma_i=0$), the τ_f* and the η_a become two constants for a given concrete and a certain normal stress σ_n. In this case, Eq. (4.15) can be simplified into the form of Bingham model, as shown in Eq. (4.16).

$$\tau = \tau_f + \frac{\eta}{\cos\theta_f}\dot{\gamma} \quad when\ \tau>\tau_f \tag{4.16}$$

Moreover, in the viscoplastic flow state, the average PCA continues to decrease with the shear flow. When the shear deformation (γ_i) reaches a certain large value, the $\theta\ (=\theta_f\cdot e^{\kappa\cdot\gamma_i})$ approaches to zero, i.e. the flocculated particle structure is completely broken down, Eq. (4.15) can be changed as the Eq. (4.17) that is also in form of Bingham model.

$$\tau = \tau_b + \eta\dot{\gamma}$$

$$\tau_b = \sigma_n\tan\phi + C_{w1} \tag{4.17}$$

For high fluidity concrete, if ignoring its granular characteristics, its average PCA can be regarded as zero, i.e.$\theta_f = 0$. Eq. (4.17) can also be obtained from Eq. (4.15) to describe the flow behavior of high fluidity concrete. The Bingham yield stress τ_b is only related to inter-friction caused be normal stress and capillary pressure of pore water. That is to say, from Eq. (4.15), the rheological model of high fluidity concrete can be derived.

Overall, if not considering the effects of stress duration or shearing time ($t=0$) and particle configuration ($\theta_f=0$), or when the flocculated particle structure of fresh concrete is completely broken down ($\theta_f\cdot e^{\kappa\cdot\gamma_i}\rightarrow 0$), The Bingham model equation can be deduced from Eq. (4.15). That is to say, Bingham model is a special model not considering the granular characteristics of fresh concrete. The reliability of Eq. (4.15) was indirectly confirmed by the derivation of the Bingham model equation.

5. Numerical analysis of shear deformation and flow behaviors based on the constitutive equations

5.1. Shear stress-shear strain, shear rate relationships

In the following, using the constitutive equations obtained by the microscopic approach, the shear deformation and flow behaviors were analyzed to investigate the effects of concrete fluidity, normal stress, and loading rate, in addition to validating the constitutive equations by comparing with the experimental results. After the parameter study, the parameter values related to a concrete mixture were set up, as shown in Table 2. The environmental temperature was 20 °C (T = 293k). Other parameter values in the constitutive equations, which are not shown in Table 2, were calculated on basis of Table 2, or set up as the analysis conditions that are given in the figures of numerical results. This numerical analysis was for the stress-controlled stress growth test in the viscoelastic deformation (VED) state, and the rate-controlled stress growth test in the viscoplastic flow (VPF) state, thus Eqs. (4.8), (4.9) and (4.15) were used.

Fig. 13 shows the shear stress-shear strain, shear rate relational curves under different loading speeds (s_1) in the VED state, and different shear rate accelerations (s_2) in the VPF state. As shown in Fig.13 (a) and (b), the shear strain increases with increasing shear stress, and the shear strain changes from a rapid increase stage to a slow increase stage, then a secondary rapid increase stage with increasing shear stress. Fig. 13 (c) shows that the shear rate first increases, then decreases with increasing shear stress in the VED state, and Fig. 13 (d) shows that the shear rate increases rapidly with increasing shear stress in the VPF state, exhibiting the shear thinning behavior. The down-curve of flow curve was also calculated for 0.8 $1/s^2$ of shear rate acceleration, which is a straight line, as shown in Fig. 13(d). These numerical results meet with the experimental results shown in Figs. 2 and 4.

About the effects of s_1 and s_2, Fig. 13 (b), (c) indicate that in the VED state, the larger the s_1, the smaller the shear strain, but the larger the shear rate for a given shear stress. The numerical results of the shear stress-shear rate relationship meet with the experimental results shown in Fig. 5 (b, lower). The shear deformation of fresh concrete is dependent of stress duration, and a longer lasting time of shear stress should yield a larger shear deformation. Thus, in case of large s_1, every shear stress lasts a short time so as to result in a small shear strain. However, the experimental results show that the larger the loading speed s_1, the larger the shear strain (see Fig. 9 (b, upper)), which are inconsistent with the numerical results for unknown reason, probably because that in the case of small shear strains, their order of magnitude is easily confused by measurement error. From general knowledge, the numerical results of the effect of loading speed should be correct. On the other hand, in the VPF state, for a given shear rate, the larger the s_2, the larger the shear stress, as shown in Fig. 13 (d). From the shape of flow curve, the shear thinning behavior is more noticeable for larger shear rate acceleration s_2.

Fig. 14 shows the effects of concrete's fluidity on the shear strain and the shear rate. The level of fluidity is expressed by the average interparticle friction angle (ϕ) and the initial average PCA (θ_0). For actual concrete, both the values of ϕ and θ_0 may not be equal, but for the convenience of setting up the values, the same values were used for them in the numerical calculations. The larger the values of ϕ and θ_0, the lower the concrete fluidity. In addition, if the measurement is continuous from the VED state to the VPF state, the initial average PCA of the VPF state should be θ_f. However, in order to investigate the effect of fluidity on the flow curve of the VPF state, different values of θ_f were used, the smaller the θ_f, the higher the fluidity of fresh concrete. As shown in Fig. 14, with increasing the fluidity of concrete, i.e. decreasing the values of ϕ, θ_0 and θ_f, the shear strain and the shear rate in the VED state increase for a given shear stress, and the shear stress in the VPF state decreases for a given shear rate. The higher the fluidity, the closer the flow curve in the VPF state is to a straight line, as shown in Fig. 14 (c). From Fig. 14 (b), it is found that the peak shear rate in the VED state, increases with increasing concrete fluidity. The shear stress corresponding to the peak shear rate, i.e. LPS limit stress, also increases very slightly with increasing concrete fluidity. This may be because that larger peak shear rate results in a larger viscous resistance.

Fig. 15 shows the effects of normal stress (σ_n) on the shear strain and shear rate of the fresh concrete. With increasing the σ_n, the shear strain and the shear rate in the VED state decrease for a given shear stress, and the shear stress in the VPF state increases for a given shear rate. From Fig. 15 (b), both the shear thickening and the shear thinning are found in the LPS phase, which were observed in the experiments (see Figs. 2 and 4). When the σ_n is small, fresh concrete exhibits the shear thinning behavior in the LPS phase.

The change of shear stress with time under a certain shear rate is shown in Fig. 16. As commonly understood [17], the shear stress decreases with the elapsed time, and the greater the shear rate, the faster the shear stress decreases. In summary, the numerical results show the same rheological behaviors as observed in the experiments or as generally recognized, thus the constitutive equations obtained in this study are reliable.

5.2. Whole flow curve based on the constitutive equations

Based on Eqs. (4.3) and (4.15), Fig. 17 shows the whole τ–$\dot{\gamma}$ relational curve, and the down-curve (straight line) measured after the tight particle structure was completely broken down. The basic viscosity in Eq. (4.15) is the same to the plastic viscosity of Bingham model.

The rheological behaviors of fresh concrete in the VED state and the VPF state, shown in Fig. 17, can be explained as follows.

Because the displacement of binder particle is time-dependent, the more the moving binder particles, the larger the shear rate. The moving binder particles acceleratedly increases with increasing shear stress due to the de-flocculation of binder particles and the initial loose particle structure, which causes the increase of shear rate with shear stress, called acceleration effect here, However, in the VED state, the particle configuration is tightened with the particle movement to resist the shear stress, which reduces the portion (τ_v) of shear stress used to overcome the viscous resistance of moving binder particles, and accordingly causes the decrease in the number of moving binder particles and further in the shear rate, here called deceleration effect.

In the derivation process of Eq. (4.1), as shown in Appendix, the acceleration effect was reflected by the hyperbolic function according to the Eyring's rate process theory (see Eq. (3.8)), while the deceleration effect was expressed by the increase of average PCA with shear stress (see the first equation of Eq. (3.6)). The relative magnitude of the two opposite effects determines the shear stress-shear rate relational curve in the VED state. When the acceleration effect is greater than the deceleration effect, the shear rate increases with increasing shear stress (the LPS phase). On the contrary, the shear rate decreases with increasing shear stress (the CPS phase). Not only the concrete fluidity, but also the normal stress has an effect on the relative magnitude of the two effects. In the LPS phase, though the shear rate increases with the increase of shear stress, the shear thinning and the shear thickening were observed in the experiments (see Figs. 2 and 4). Mari et al. [23] explained that strong interparticle friction leads to the shear thickening behavior of suspension. A larger θ will cause a greater frictional resistance (see Eq. (3.7)). Hence, the shear thickening is attributed to that the increase of the deceleration effect with shear stress is slightly faster than that of the acceleration effect.

On the other hand, in the VPF state, there are not only the de-

Table 2
Setting of parameters related to concrete mixture.

N ($1/m^2$)	N_c ($1/m^2$)	θ_f (deg.)	E (kT)	Λ_0 (m)	C_{w2} (Pa)	κ
9E+12	7E+12	55	21.5	5E-11	10	2E-04

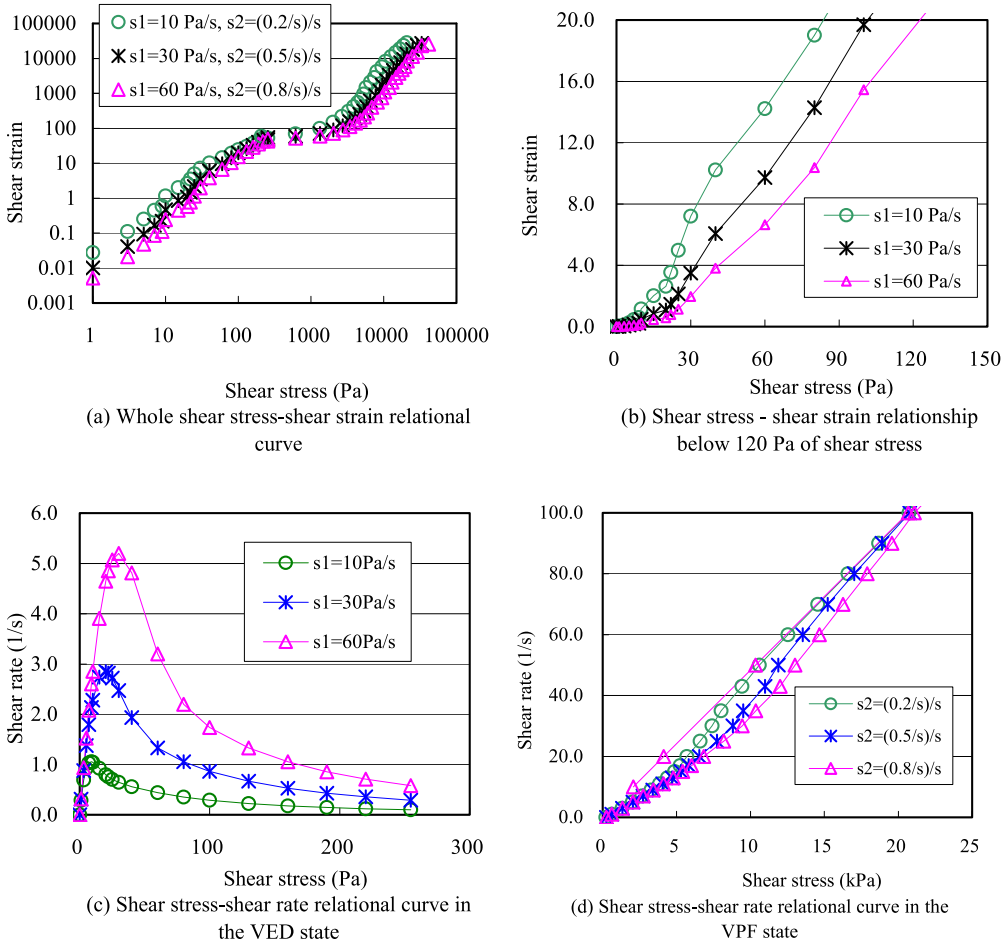

Fig. 13. Effects of loading speed (s_1) and acceleration of shear rate (s_2) on the shear strain, shear rate-shear stress relationships ($\phi = \theta_0 = 10$ deg., $\sigma_n = 100$ Pa).

flocculation of binder particles, but also the loosening of particle configuration because the jamming or interlocking of aggregate particles is broken, i.e. the average PCA decreases, thus the shear thinning behavior is present. The second equation of Eq. (3.6) was used for the derivation of Eq. (4.15) to reflect the stress-induced loosening effect of particle configuration. For high fluidity concrete, the initial particle configuration is loose, the stress-induced loosening effect is very small even none, thus the shear thinning is unnoticeable or absent.

The shear thickening of the self-compacting concretes (SCC), which had very small yield stress even negative value [11,13], was found in the rheological tests. This may be explained as a behavior in the LPS phase of the VED state, where the particle configuration is loose. The tightness of particle configuration gradually increases with increasing the shear stress, but the SCC remains in the LPS phase due to obvious suspension characteristic. It was reported that the shear thickening also happens at relatively high shear rates in suspensions [23]. The explanation for this phenomenon is that at a certain high shear rate, the shear force that pushes the particles together becomes large, thus easily creates a frictional contact network, i.e. the increase of the deceleration effect is faster than the increase of the acceleration effect. Overall, for understanding the rheological behaviors of fresh concrete, the particle contact and the variation of particle contact tightness with shear deformation should be noticed.

For using the constitutive equations to perform the numerical flow simulation of fresh concrete [42], the author has already developed a parallel plate type rheometer, called RSNS (Ring Shear under Normal Stress) rheometer, and proposed the test methods for the parameters of the constitutive equations [58]. The RSNS rheometer was fabricated by improving the rheometer shown in Fig. 3. An electric motor replaced the air motor to drive the lower rotating blade, and allowed a continuous measurement from stress-controlled stress growth to shear rate growth. Two air cylinders are used to apply vertical pressure on concrete sample's top surface to investigate the effect of normal stress.

The time-dependence of the rheological property, so called thixotropy, of fresh concrete is not only associated with the stress history that affects the physical flocculation-dispersion of particles, but also the elapsed time from mixing up [59] that is related to cement hydration. However, because of the complexity of influencing factors of cement hydration rate, it is not an easy work to model the rheological behaviors of fresh concrete considering the elapsed time. For this reason, numerical analysis is an alternative tool for predicting thixotropy [60].

6. Summary

In this paper, a theoretical analysis method, called microscopic approach, was used to investigate and model the rheological properties of fresh concrete. Fresh concrete was regarded as a granular fluid composed of water, viscous binder particles, and non-viscous aggregate particles. The granular characteristics were represented by interparticle frictional angle (ϕ) and particle contact angle (PCA). Average PCA can quantify the tightness of particle configuration. The shear deformation was derived by

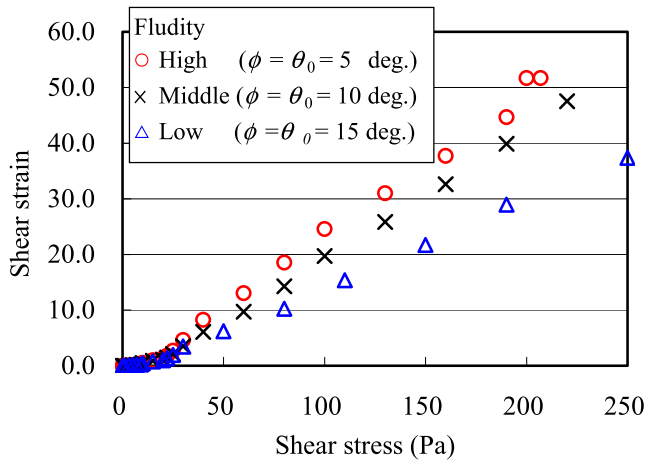

(a) Shear stress-shear strain relationship in the VED state

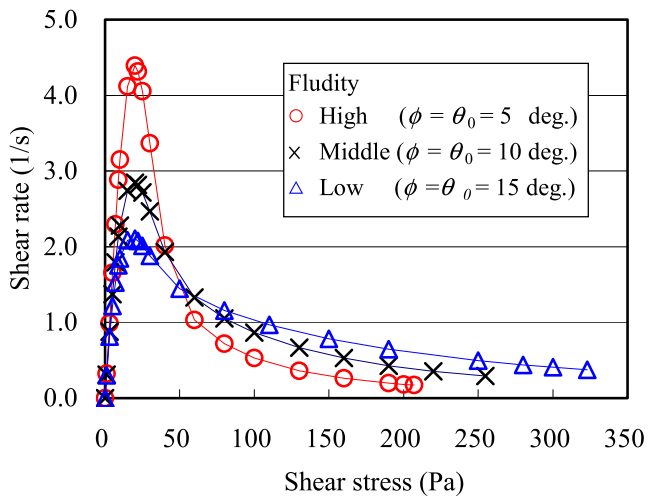

(b) Shear stress-shear rate relationship in the VED state

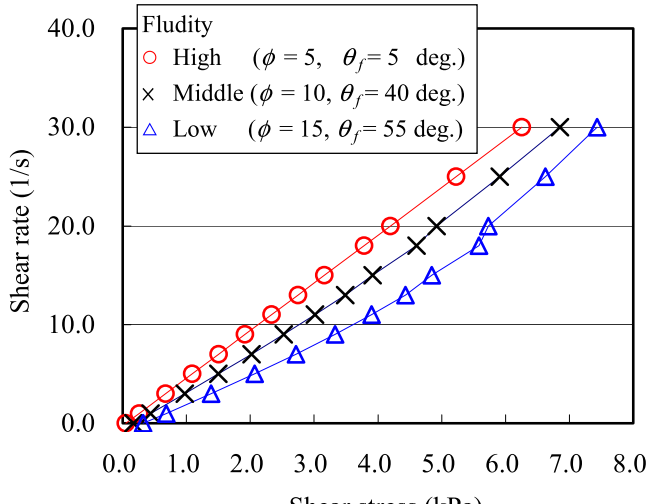

(c) Shear stress-shear rate relationship in the VPF state

Fig. 14. The shear strain, shear rate-shear stress relationships of fresh concrete with different fluidity ($s_1 = 30$ Pa/s, $s_2 = 0.2/s^2$, $\sigma_n = 100$ Pa).

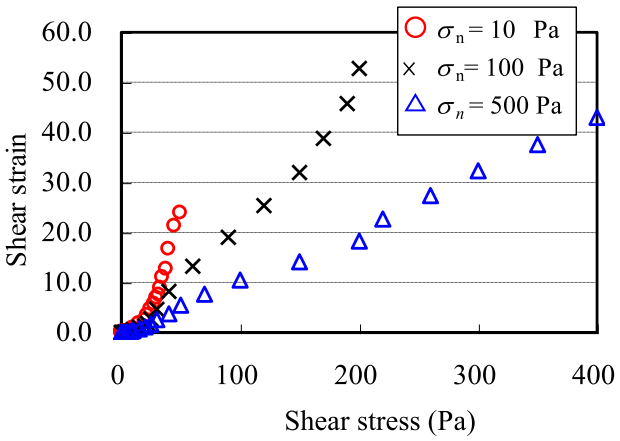

(a) Shear stress-shear strain relationship in the VED state

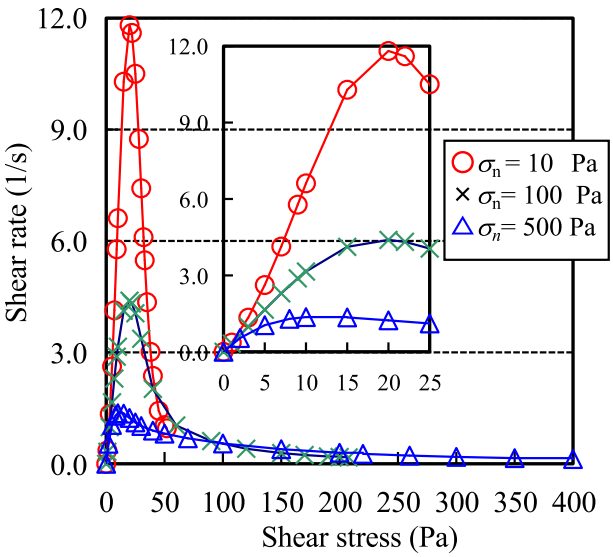

(b) Shear stress-shear rate relationship in the VED state

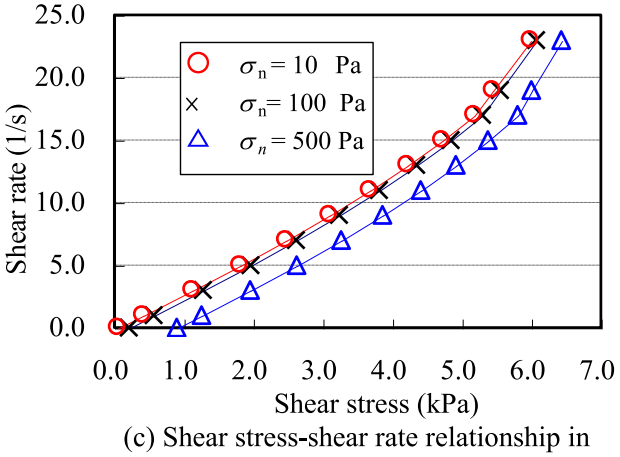

(c) Shear stress-shear rate relationship in the VPF state

Fig. 15. Effects of normal stress on the shear strain, shear rate-shear stress relationships ($s_1 = 30$ Pa/s, $s_2 = 0.2/s^2$, $\phi = \theta_0 = 5$ deg.).

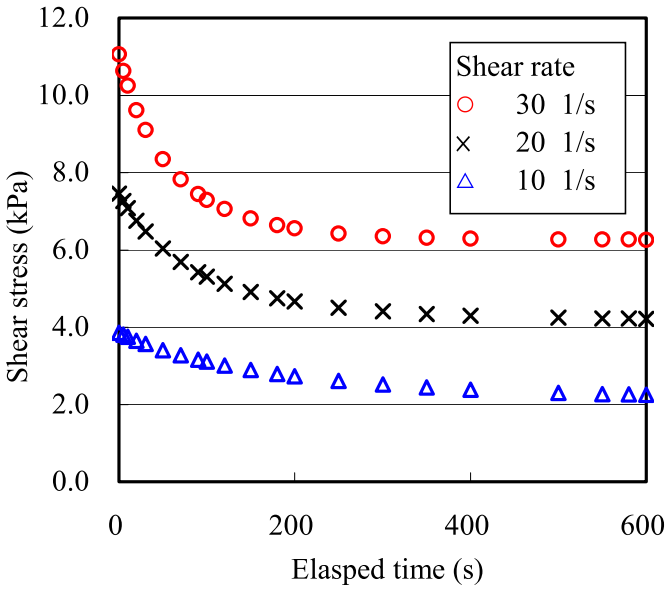

Fig. 16. Variation of shear stress with elasped time at a certain shear rate ($\phi = 10$ deg., $\sigma_n = 100$ Pa).

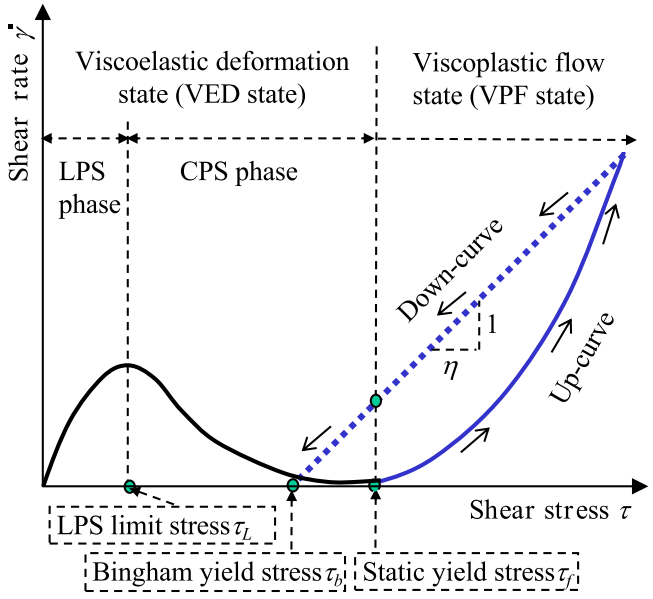

Fig. 17. Whole flow curve of fresh concrete.

accumulating the particle motions in the shear direction.

Appendix. Derivation of Eq. (4.1)

For granular materials containing only non-viscous particle (e.g. sand and gravel), if the interparticle force can overcome simultaneously the interfraction and dilatancy resistances of a particle, the particle will migrate. According to Eq. (3.5) and the first equation of Eq. (3.6), the probability (P_t) of occurrence of moving particles before yielding is expressed by Eq. (A.1), where C_{w2} is a function of capillary pressure of water and depends on the θ, but can be approximated as a constant here because it is small.

$$P_t = \frac{\tau}{2(\sigma_n + C_{w2})\left(\phi + \theta_0 + \frac{\theta_f - \theta_0}{\tau_f}\tau\right)} \tag{A.1}$$

Where, $C_{w2} = Nf_{wm}\cos\theta$

With the increase of shear stress, fresh concrete behaves from the viscoelastic deformation (VED) state to the viscoplastic flow (VPF) state. The constitutive equations were obtained respectively for the two states, as shown in Eqs. (4.1), (4.3) and (4.15), by using the microscopic approach. And the static yield stress model is expressed by Eq. (4.11). Whole flow curve of fresh concrete before and after yielding is shown in Fig. 17.

Due to the consideration of the frictional resistance and the dilatancy resistance caused by the ϕ, and the PCA, respectively. The no-linear, normal stress-dependent, and shear thinning characteristics of the visco-plastic flow of fresh concrete can be reflected in the constitutive equation Eq. (4.15). If not considering the particle configuration, the Bingham model equation can be derived from the Eq. (4.15), and the Bingham yield stress is associated with the interparticle friction (see Eq. (4.17)).

The viscoelastic deformation state contains the loose particle structure phase (LPS phase) and the close particle structure phase (CPS phase). With the increase of shear stress, the shear stain increases rapidly in the LPS phase, whereas in the CPS phase the shear stain increases slowly, and the shear rate decreases due to the fast particle configuration tightening.

The numerical calculations based on the constitutive equations showed that the obtained rheological models can describe the complex rheological behaviors of fresh concrete observed in the rheological experiments, and are applied to the fresh concretes from stiff to high fluidity types.

Author statement

Zhuguo Li: Conceptualization, Methodology, Investigation, Validation, Writing - Original, Writing - Review & Editing.

Declaration of competing interest

The authors declare that they have no known competing financial interests or personal relationships that could have appeared to influence the work reported in this paper.

Data availability

No data was used for the research described in the article.

Acknowledgments

The author would like to thank Dr. Yasuo Tanigawa, Professor Emeritus of Nagoya University, for his direction, and Mr. Minoru Iidaka, Technical Staff of Tsukuba University, for his assistance in the fabrication of the rheometers.

Substituting Eq. (A.1) and the first equation of Eq. (3.10) into Eq. (3.9), the shear strain (γ^*) of non-viscous granular material before yielding can be gotten as Eq. (A.2).

$$\gamma^* = NP_t\frac{\Lambda_0}{\cos\theta}\cos\theta = \frac{c_1\tau}{c_2 + c_3\tau} \tag{A.2}$$

where, $c_1 = \frac{N\Lambda_0}{2(\sigma_n + C_{w2})}$, $c_2 = \phi + \theta_0$, $c_3 = \frac{\theta_f - \theta_0}{\tau_f}$

However, for fresh concrete, some of shear stress is used to overcome the viscous resistance (τ_v) exposed to the moving binder particles. Thus, the shear strain of fresh concrete in the viscoelastic deformation state should be represented by Eq. (A.3).

$$\gamma = \frac{c_1(\tau - \tau_v)}{c_2 + c_3(\tau - \tau_v)} \tag{A.3}$$

Substituting Eq. (A.4) into Eq. (A.3), Eq. (A.5) can be obtained.

$$\tau - \tau_v = G\gamma \tag{A.4}$$

where, G is secant modulus of elasticity.

$$G = \frac{c_2}{c_1 - c_3\gamma} \tag{A.5}$$

By differentiating both sides of Eq. (A.5) with respect to time t, and then substituting Eq. (A.3) into it, Eq. (A.6) was obtained. And from Eqs. (A.4) and (A.5), Eq. (A.7) was derived.

$$\frac{dG}{dt} = \frac{c_3}{c_1^2 c_2}[c_2 + c_3(\tau - \tau_v)]^2\frac{d\gamma}{dt} \tag{A.6}$$

$$\tau_v = \tau - \frac{c_1 G - c_2}{c_3} \tag{A.7}$$

After differentiating both sides of Eq. (A.7) with respect to time t and substituting Eq. (A.6) into it, Eq. (A.8) was obtained.

$$\frac{d\tau_v}{dt} = \frac{1}{c_1 c_2}[c_2 + c_3(\tau - \tau_v)]^2\frac{d\gamma}{dt} \tag{A.8}$$

As explained above, the viscous resistance τ_v occurs only when the binder particles migrate, and the interparticle force works first to overcome the shear resistance τ^*. The probability (P_{tc}) of occurrence of the active binder particles in the viscoelastic deformation state is expressed by Eq. (A.9) according to Eq. (A.1).

$$P_{tc} = \frac{\tau}{2(\sigma_n + C_{w2})(c_2 + c_3\tau)} \tag{A.9}$$

After substituting Eq. (3.8), the first equation of Eq. (3.10) and Eq. (A.9) into Eq. (3.11), following by substituting Eq. (3.11) into Eq. (A.8), Eq. (A.8) was changed as Eq. (A.10).

$$\frac{d\tau_v}{dt} = -\frac{1}{c_1 c_2}[c_2 + c_3(\tau - \tau_v)]^2 \cdot \frac{2A\Lambda_0 c_4\tau}{(c_2 + c_3\tau)}\sinh\left[\frac{c_5(c_2 + c_3\tau)}{c_4\tau}\tau_v\right] \tag{A.10}$$

where, $c_4 = \frac{N_c}{2(\sigma_n + C_{w2})}$, $c_5 = \frac{\Lambda_c}{2kT}$

Integrating Eq. (A.10) for time t, Eq. (A.11) was obtained.

$$\tau_v = \frac{\tau(c_2 + c_3\tau)}{c_2\exp(qt) + c_3\tau}$$

$$q = \frac{2\Lambda_c(\sigma_n + C_{w2})(c_2 + c_3\tau)^2}{hNL_0^{-2}(\phi + \theta_0)\exp(E/kT)} \tag{A.11}$$

Substituting Eq. (A.11) into Eq.(A.3), the shear strain equation of fresh concrete in the VED state was obtained, as shown in Eq. (4.1).

References

[1] Architectural Institute of Japan (AIJ). Japanese architectural standard specification: JASS 5 reinforced concrete work. 2015. p. 183–5 [in Japanese].

[2] Ferraris CF, Billberg P, Ferron R, Feys D, Hu J, Kawashima S, Tanesi J, Tregger N. Role of rheology in achieving successful concrete performance. Concr Int 2017;39:43–51.

[3] Zhao Z, Chen M, Jin Y, Lu L, Li L. Rheology control towards 3D printed magnesium potassium phosphate cement composites. Compos B Eng 2022;239:109963.

[4] Cho S, Kruger J, van Rooyen A, van Zijl G. Rheology and application of buoyant foam concrete for digital fabrication. Compos B Eng 2021;215:108800.

[5] Chen M, Liu B, Li L, Cao L, Huang Y, Wang S, et al. Rheological parameters, thixotropy and creep of 3D-printed calcium sulfoaluminate cement composites modified by bentonite. Compos B Eng 2020;186:107821.

[6] Tanigawa Y, Mori H. Towards establishment of 'workability design method' for concrete. Cem Concr 1988;501:11–20 [in Japanese].

[7] Tattersall GH. The rationale of a two-point workability test. Mag Concr Res 1973;25(84):169–72.

[8] Koehler EP, Fowler DW. Development of a portable rheometer for fresh portland cement concrete, Report of International Center for Aggregates Research. The University of Texas at Austin; 2004. p. 57–176. No. ICAR105-3F.

[9] De Larrard F, Ferraris CF, Sedran T. Fresh concrete: a Herschel-Bulkley material. Mater Struct 1998;31(211):494–8.

[10] Papo A. Rheological models for cement pastes. Mater Struct 1988;21(1):41–6.

[11] Feys D, Verhoeven R, De Schutter G. Fresh self compacting concrete, a shear thickening material. Cement Concr Res 2008;38(7):920–9.

[12] Li Z, Ohkubo T, Tanigawa Y. Flow performance of high-fluidity concrete. J Mater Civ Eng 2004;16(6):588–96.

[13] Feys D, De Schutter G, Verhoeven R. The rheological behaviour of fresh self-compacting concrete in the high shear rate range. In: RILEM bookseries, vol. 2. Dordrecht, The Netherlands: Springer; 2010. p. 491–501. https://biblio.ugent.be/publication/1170093.
[14] Rubio-Hernández F-J. Rheological behavior of fresh cement pastes. Fluid 2018;3(106):1–16.
[15] Shi Y, Matsui I, Feng N. Effect of compound mineral powders on workability and rheological property of HPC. Cement Concr Res 2002;32(1):71–8.
[16] Banfill PFG. Rheology of fresh cement and concrete. In: Rheology reviews. British Society of Rheology; 2006. p. 61–130.
[17] Assaad J, Khayat KH, Mesbah H. Assessment of thixotropy of flowable and self-consolidating concrete. Mater J 2003;100(2):99–107.
[18] Mahaut F, Mokeddem S, Chateau X, Roussel N, Ovarlez G. Effect of coarse particle volume fraction on the yield stress and thixotropy of cementitious materials. Cement Concr Res 2008;38(11):1276–85.
[19] Geiker MR, Brandl M, Thrane LN, Bager DH, Wallevik O. The effect of measuring procedure on the apparent rheological properties of self-compacting concrete. Cement Concr Res 2002;32(11):1791–5.
[20] Li Z, Ohkubo T, Tanigawa Y. Theoretical analysis of time-dependence and thixotropy of fluidity for high fluidity concrete. J Mater Civ Eng 2004;16(3):247–56.
[21] Vom Berg W. Influence of specific surface and concentration of solids upon the flow behaviour of cement pastes. Mag Concr Res 1979;31(109):211–6.
[22] Stickel JJ, Powell RL. Fluid mechanics and rheology of dense suspensions. Annu Rev Fluid Mech 2005;37(1):129–49.
[23] Mari R, Seto R, Morris JF, Denn MM. Shear thickening, frictionless and frictional rheologies in non-Brownian suspensions. J Rheol 2014;58(6):1693–724.
[24] Yammine J, Chaouche M, Guerinet M, Moranville M, Roussel N. From ordinary rheology concrete to self compacting concrete: a transition between frictional and hydrodynamic interactions. Cement Concr Res 2008;38(7):890–6.
[25] Li Z, Ohkubo T, Tanigawa Y. Yield model of high fluidity concrete in fresh state. J Mater Civ Eng 2004;16(3):195–201.
[26] Faroug F, Szwabowski J, Wild S. Influence of superplasticizers on workability of concrete. J Mater Civ Eng 1999;11(2):151–7.
[27] Mori H, Tanaka M, Tanigawa Y. Experimental study on shear deformation of fresh concrete. J Struct Constr Eng (Trans. of AIJ) 1991;421:1–10 [in Japanese].
[28] Roussel N, Bessaies-Bey H, Kawashima S, Marchon D, Vasilic K, Wolfs R. Recent advances on yield stress and elasticity of fresh cement-based materials. Cement Concr Res 2019;124:105798. https://doi.org/10.1016/j.cemconres.2019.105798.
[29] Nachbaur L, Mutin JC, Nonat A, Choplin L. Dynamic mode rheology of cement and tricalcium silicate pastes from mixing to setting. Cement Concr Res 2001;31:183–92.
[30] Roussel N. A thixotropy model for fresh fluid concretes: theory, validation and applications. Cement Concr Res 2006;36:1797–806.
[31] Struble LJ, Schultz MA. Using creep and recovery to study flow behavior of fresh cement paste. Cement Concr Res 1993;23:1369–79.
[32] Li Z, Li J. Experimental study on shear deformation of fresh concrete. J Struct Constr Eng (Trans. of AIJ) 2010;75:1173–80 [in Japanese].
[33] Roussel N, Ovarlez G, Garrault S, Brumaud C. The origins of thixotropy of fresh cement pastes. Cement Concr Res 2012;42:148–57.
[34] Barnes HA. The yield stress—a review or ‘παντα ρει’—everything flows? J Nonnewton Fluid Mech 1999;81:133–78.
[35] Ovarlez G, Roussel N. A physical model for the prediction of lateral stress exerted by self-compacting concrete on formwork. Mater Struct 2006;39:269–79.
[36] Qian Y, Kawashima S. Distinguishing dynamic and static yield stress of fresh cement mortars through thixotropy. Cem Concr Compos 2018;86:288–96.
[37] Saak AW, Jennings HM, Shah SP. The influence of wall slip on yield stress and viscoelastic measurements of cement paste. Cement Concr Res 2001;31:205–12.
[38] Tattersall GH, Dimond CR. The use of the coaxial cylinders viscometer to measure the rheological properties of cement pastes, Hydraul Cem Pastes: Struct and Properties. Cem Concr Assoc, Slough 1976;15:118–33.
[39] Bhatty JI, Banfill PFG. Sedimentation behaviour in cement pastes subjected to continuous shear in rotational viscometers. Cement Concr Res 1982;12:69–78.
[40] Wallevik JE. Rheology of particle suspensions: fresh concrete, mortar and cement paste with various types of lignosulfonates. Ph. D Thesis of Norwegian Univ of Sci and Tech; 2003. p. 11–47.
[41] Li J, Li Z. Effect of boundary restraint on flow of fresh concrete though opening. J Struct Constr Eng (Trans. of AIJ) 2011;76:1367–74 [in Japanese].
[42] Cao G, Li Z, Xu Z. A SPH simulation method for opening flow of fresh concrete considering boundary restraint. Construct Build Mater 2019;198:379–89.
[43] Brower LE, Ferraris CF. Comparison of concrete rheometers. Concr Int 2003;25:41–7.
[44] Soualhi H, Kadri E-H, Ngo T-T, Bouvet A, Cussigh F, Kenai S. A vane rheometer for fresh mortar: development and validation. Appl Rheol 2014;24:1–7.
[45] Ferraris CF, Li Z, Zhang M-H, Stutzman P. Development of a reference material for the calibration of cement paste rheometers. Adv Civ Eng Mater 2013;2:140–62.
[46] Murayama S. Theory of mechanical behavior of soil. Gihodo Publishing; 1990. p. 27–375 [in Japanese].
[47] Li Z, Tanigawa Y, Mori H, Kurokawa Y. Study on constitutive law of fresh mortar based on particle assembly model. J Struct Constr Eng (Trans. of AIJ) 1999;523:17–24 [in Japanese].
[48] Li Z, Cao G. Rheological behaviors and model of fresh concrete in vibrated state. Cement Concr Res 2019;120:217–26.
[49] Uzomaka OJ. A concrete rheometer and its application to a rheological study of concrete mixes. Rheol Acta 1974;13:12–21.
[50] Li Z, Li J, Zhang W. Mechanical responses of freshly mixed cementitious materials to small and slow shear deformation. Proc Japan Concr Inst 2009;31:1441–6.
[51] Li Z, Li J, Iidaka M. Development of rheometer of fresh concrete for stress-controlled stress growth test. Proc Japan Concr Inst 2011;33:1211–6 [in Japanese].
[52] Li Z, Kajiwara K, Iidaka M. Investigation on particle contact angle of fresh concrete using X-ray CT imaging. J Society of Mater Sci, Japan 2013;62:585–91 [in Japanese].
[53] Li Z, Tanigawa Y. Investigation on granular characteristics of fresh concrete based on visualized experiment using alternative materials. J Struct Constr Eng (Trans. of AIJ) 2012;77:1175–84 [in Japanese].
[54] Mishima N, Tanigawa Y, Mori H, Kurokawa Y, Terada K, Hattori T. Experimental study on rheological properties of dense suspension by shear box test. J Struct Constr Eng (Trans. of AIJ) 2000;65:13–9 [in Japanese].
[55] Li Z, Ohkubo T, Mori H, Tanigawa Y. A theoretical study on viscoplastic shear deformation behavior of fresh concrete. J Struct Constr Eng (Trans. of AIJ) 2003;564:1–8 [in Japanese].
[56] Li Z. A theoretical study on the bleeding model of fresh concrete in static state. J Struct Constr Eng (Transactions of AIJ) 2012;77:1357–66 [in Japanese].
[57] Li Z, Li J. Granular material characteristic of fresh concrete. In: Proc of 6th inter RILEM symp. on self-compacting concr, Montreal, Canada; 2010. p. 423–33.
[58] Li Z, Iidaka M. Development of rheological measurement method for fresh concrete considering its granular characteristic. In: Proc of 6th inter confer on constr mat: performance, innovations and structural implications, Fukuoka, Japan; 2020. p. 1456–67.
[59] Shaughnessy III R, Clark PE. The rheological behavior of fresh cement pastes. Cement Concr Res 1988;18:327–41.
[60] Li Z, Cao G, Guo K. Numerical method for thixotropic behavior of fresh concrete. Construct Build Mater 2018;187:931–41.